TRIBOLOGICAL CHARACTERIZATION OF CARBON BASED SOLID

LUBRICANTS

A Thesis

by

CARLOS JOEL SANCHEZ

Submitted to the Office of Graduate Studies of
Texas A&M University
in partial fulfillment of the requirements for the degree of

MASTER OF SCIENCE

August 2011

Major Subject: Mechanical Engineering

TRIBOLOGICAL CHARACTERIZATION OF CARBON BASED SOLID LUBRICANTS

A Thesis

by

CARLOS JOEL SANCHEZ

Submitted to the Office of Graduate Studies of
Texas A&M University
in partial fulfillment of the requirements for the degree of

MASTER OF SCIENCE

Approved by:

Chair of Committee,	Hong Liang
Committee Members,	Bing Guo
	Michael Pate
Head of Department,	Jerald Caton

August 2011

Major Subject: Mechanical Engineering

ABSTRACT

Tribological Characterization of Carbon Based Solid Lubricants.

(August 2011)

Carlos Joel Sanchez, B.S., Texas A&M University

Chair of Advisory Committee: Dr. Hong Liang

High performance machines such as gas turbine engines demand efficient solid lubricants at high temperature and in vacuum. The current conventional solid lubricants need to be further improved. This research evaluates carbon based solid lubricants using a high vacuum, high temperature pin-on-disc tribometer. The objectives of this research were to develop an understanding of the tribological properties of solid lubricant coatings under extreme operating conditions, and to determine whether using a carbon based solid lubricant would be acceptable for use in those conditions.

Experimentally, two solid lubricant coatings on tungsten carbide substrate were tested against two different materials. The coatings were carbon based and molybdenum disulfide based. The other materials were 440C stainless steel and tungsten carbide. The temperature, pressure, and relative humidity are independent variables. The results showed that the carbon based coating increases friction and wears out quickly due to high temperature, high vacuum, and low humidity. Abrasive wear is the dominating mechanism. At elevated temperatures and in dry environment, the carbon based coating underwent significant oxidation and phase transformation. This research is beneficial for

future design and development of solid lubricants for aerospace applications, as well as other industries requiring lubricants that must operate in extreme conditions.

This thesis includes five chapters. Chapter I is an introduction to tribology and to the materials being used in this research. Chapter II describes the motivation and objectives behind this research. Chapter III discusses the experimental procedure and further explains the materials used. Chapter IV presents and discusses the results obtained. Chapter V discusses the major conclusions obtained from the results and offers some future work that may be conducted concerning this research.

ACKNOWLEDGEMENTS

I would like to thank my committee chair and advisor, Dr. Hong Liang, for all her support and guidance throughout the course of my research. I have also received a lot of help and guidance from the students in the Liang Surface Science Research Group throughout my graduate studies. I would also like to thank my committee members, Dr. Michael Pate and Dr. Bing Guo, for their support and Dr. Robert Bruce, from GE Aviation, for giving me the opportunity to work on this research project. I am also grateful for the scholarship awarded to me by the STLE Houston chapter to continue my research and interest in tribology.

Most importantly, I would like to thank my parents, Carlos and Bertha Sanchez, for all of their support throughout my academic career. They have made a lot of sacrifices throughout the years to send to Texas A&M so that I may reach my goal of becoming a mechanical engineer. I would not be where I am without them and I am extremely grateful. Finally, I would like to thank my fiancé for being very supportive and patient throughout the course of my research.

NOMENCLATURE

ASTM   American Society for Testing and Materials

CCD   Charge Coupled Device

EDS   Energy Dispersive X-ray Spectroscopy

GE   General Electric

HTT   High Temperature Tribometer

LCD   Liquid Crystal Display

MoS2   Molybdenum Disulfide

RPM   Revolutions per Minute

SEM   Scanning Electron Microscope

SS   Stainless Steel

SSRL   Stanford Synchrotron Radiation Light-source

STLE   Society of Tribologist and Lubrication Engineers

WC   Tungsten Carbide

XPS   X-Ray Photoelectron Spectroscopy

TABLE OF CONTENTS

LIST OF FIGURES

LIST OF TABLES

CHAPTER I

INTRODUCTION

An understanding of tribology, friction, lubrication, and wear will be established in this chapter . Solid lubricants, and carbon based coatings will also be described.

1.1. Tribology

Tribology is a science related to the study of the interaction between materials that are in relative motion. The term Tribology was first coined in Europe in 1967 by the Organization for Economic and Cooperation and Development; the root of the word coming from the Greek "tribos," meaning rubbing [1]. It is an interdisciplinary science, combining the study of lubrication, friction, and wear. Although Tribology is a relatively new form of science, its study and implications can be seen throughout recorded history.

The importance of friction study can be seen in early civilizations. Paleontologists have discovered that ancient peoples would create fire by rubbing sticks together, or by striking flint or pyrite rocks to create sparks [2]. It is also speculated that ancient Sumerians used grease-like substances to lubricate wheel axles as early as 3500 B.C [3].

Although, the importance of friction and lubrication has been known since ancient times, Leonardo Da Vinci was actually the first to elaborate on the laws of friction [4] and thus began this study as a science. Da Vinci proposed many experiments that demonstrated the effects of friction on different objects. He stated that the frictional

This thesis follows the style of *Journal of Tribology*.

force is proportional to the weight of the object and is independent of geometry [5]. However, Da Vinci's works were not published for hundreds of years and it took until 1699 [6] for Guillaume Amontons to rediscover the laws of friction. According to Amontons, friction resistance is proportional to load and independent of surface contact area [7].

Of the three tribological disciplines, wear behavior would be the most recent to be studied. When surfaces interact, they generate friction, which inherently leads to loss of material, or wear. The wear loss of materials is a critical issue in the performance of machines which have interacting components. It is of great economic importance for industries to understand material removal rates in relation to quality requirements [8]. Wearing of material has the potential to create energy loss, reduction in efficiency, and overall reduce the lifespan of a material.

Tribological study has implications in many industries including mechanical, electrical, and even computer engineering. Being able to understand and improve the way that materials interact will lead to improvements and advances in many fields.

1.2. Friction

Friction is the resistive force generated between two surfaces interacting with each other. Frictional force is a primary cause of loss of material between surfaces and can cause significant issues depending on the situation. As mentioned in the previous section, the laws of friction were first developed by Leonardo Da Vinci. These early laws were then further elaborated by Amontons. Several years later after conducting his own experiments, French physicist Charles Coulomb observed that the frictional

resistance among mating materials arose from the mechanical interlocking of surface asperities [6]. Expanding on Amontons friction laws, Coulomb also noted that friction is independent of velocity one the objects are in motion [9]. Around the same time in history, Swiss mathematician Leonhard Euler performed experiments involving inclined planes [1, 10] and developed the concepts of static and kinetic friction.

Many factors contribute to the level of frictional force, including: geometry, material properties, and environmental conditions. This thesis will focus on the analysis of lubricated friction and dry friction. Lubricated friction describes the friction in which a lubricating material is sandwiched between two moving surfaces. Dry friction describes the resistance of two solid surfaces in relative contact with one another. This type of friction can be broken up into two categories: static friction, and kinetic friction.
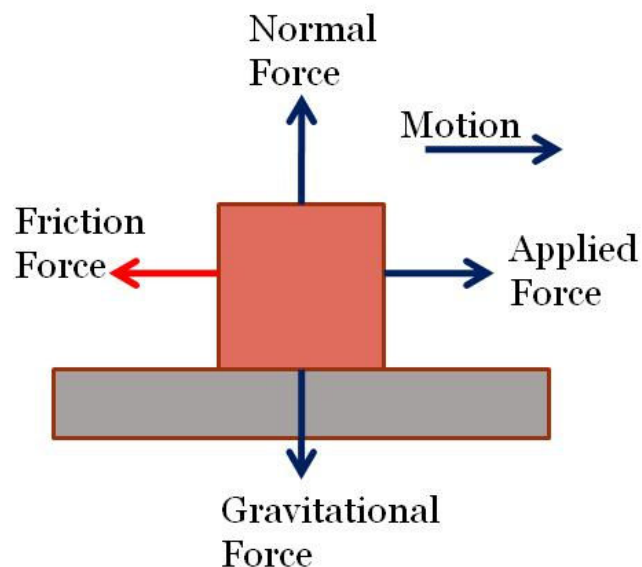
Figure 1. Model representing the various forces acting on two interacting bodies.

Static friction is the force which resists the motion of two bodies which are in contact. An example of static friction would be a large block sitting on an inclined platform. The block will remain on the platform unless the force of static friction is overcome. The amount of static friction arises from several factors including: surface geometry, electrostatic forces, mass of the objects, and even chemical interactions.

Once two objects overcome the force of static friction, another resistive force will occur; this is the force of kinetic friction. Typically, the value of kinetic friction is less than static friction. This phenomenon can be experienced when one tries to move a large piece of furniture across a room. Initially, it takes a lot more force to get the furniture in motion than it does to actually keep it in motion. However, this effect will depend on the material and rate of motion; among other factors. As seen in Figure 1, the friction force will act opposite to the direction of motion.

Other forms of friction include internal friction, fluid friction, and dry friction. Internal friction describes the resistive forces between interacting molecules at the surface. Fluid friction is the resistive force between fluids which are in motion. Dry friction refers to the resistive force between two solid objects [11].

In this thesis, the coefficient of friction will be measured to evaluate the performance of two interacting materials. The coefficient of friction is a dimensionless quantity that is measured as the ratio of the friction force to the normal force. The relationship can be seen in the following equation:

$$\mu = \frac{f}{N} \tag{1}$$

Where, f is the resistance force and N is the normal force acting on the object. A higher friction coefficient indicates that there is more force resisting the motion of two objects. The experiments being conducted in this thesis will focus on the measurement of kinetic and lubricated friction between two test materials. The method by which these values are obtained will be discussed in a later chapter.

1.3. Wear

The progressive loss of material among interacting surfaces is called wear. It occurs as a result of mechanical and/or chemical interactions, and can be accelerated by thermal means due to friction [12]. One contributing factor is the surface characteristics of the material. In addition to surface asperities, the wear volume/rate will be a function of material hardness.

This research will focus on the tribological behavior of two materials in sliding motion. The first relationships of wear resulting from sliding motion were proposed by Archard and Holm [13]. Holm's theory modeled wear as atoms being removed from the surface. Archard expanded on this theory, stating that clusters of atoms or asperities caused wear as opposed to individual atoms [14]. The relationship in Equation 2 describes the Archard-Holm Law.

$$V = \frac{K}{H}FS \tag{2}$$

Where V is the worn volume, K is the coefficient of wear, H is the material hardness, F is the applied load, and S is the sliding distance. In this equation, the wear coefficient is dependent on surface characteristics and determined experimentally.

Tribological study focuses on analyzing the mechanisms which cause wear in the hopes of improving machine performance. The mechanisms responsible for wear include, abrasive, adhesive, fretting, and tribo-chemical wear.

Abrasive wear occurs when a material begins to remove pieces from the surface of another material due to surface asperities. As shown in Figure 2, when the top material comes into contact with the bottom material, it begins to remove a small segment on the surface. In this case, the top material contains harder surface asperities which removed softer asperities on the bottom material. Once a surface particle is removed, it may remain between the two surfaces and cause additional wear of the materials, this is known as three body wear. When a hard asperity remains attached to the surface and gradually wears into the softer material, it is known as two body wear.
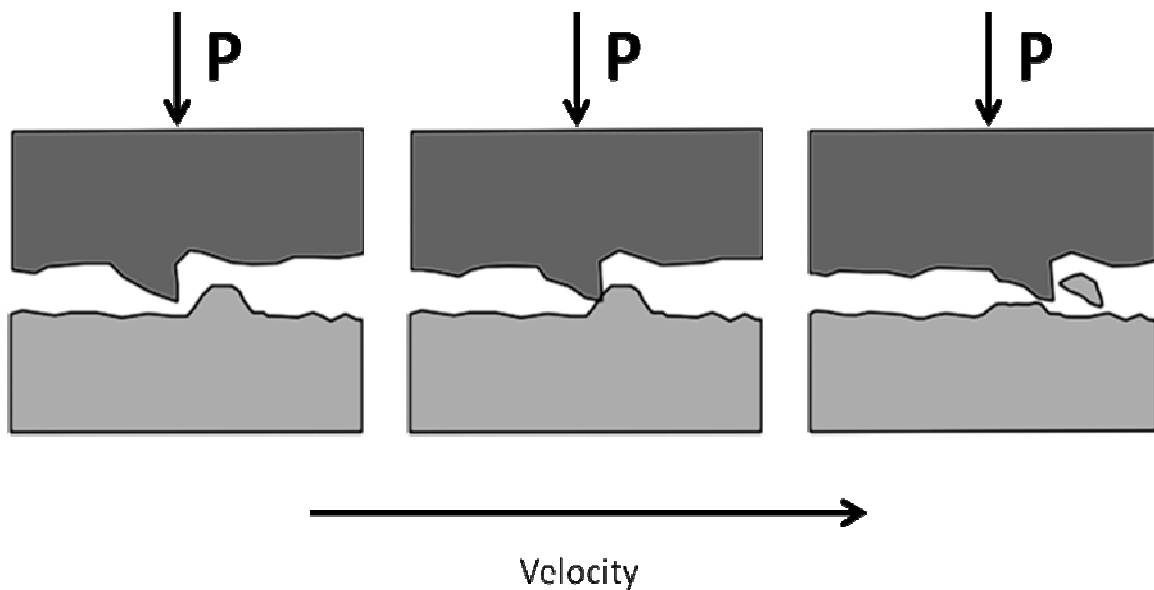
Figure 2. This figure illustrates the abrasive removal of one material by another.

As hard asperities and particles continue to slide and roll across the surface, different abrasive mechanisms will come into play. These mechanisms will include cutting, fracture, fatigue, and grain pull out [11, 12]. Cutting occurs when a hard particle ploughs across the surface of a softer material, causing plastic deformation. Fracture will occur when a hard particle begins to embed itself within the softer material, causing it to crack at the surface. Fatigue occurs as a result of repeated plastic deformation due to cutting. Finally, grain pull out occurs when a grain boundary is removed from the surface.

Adhesive wear occurs when the surface of one material "sticks" to the surface of another and is removed. As shown in Figure 3, when the top material comes into contact with the bottom material, an adhesive process occurs which will lead to a transfer of material. This process of displacement and attachment of wear debris can occur between both surfaces. The mechanism responsible for adhesive wear is electron transfer, causing adhesive bonds between the materials at the surface [1, 9].
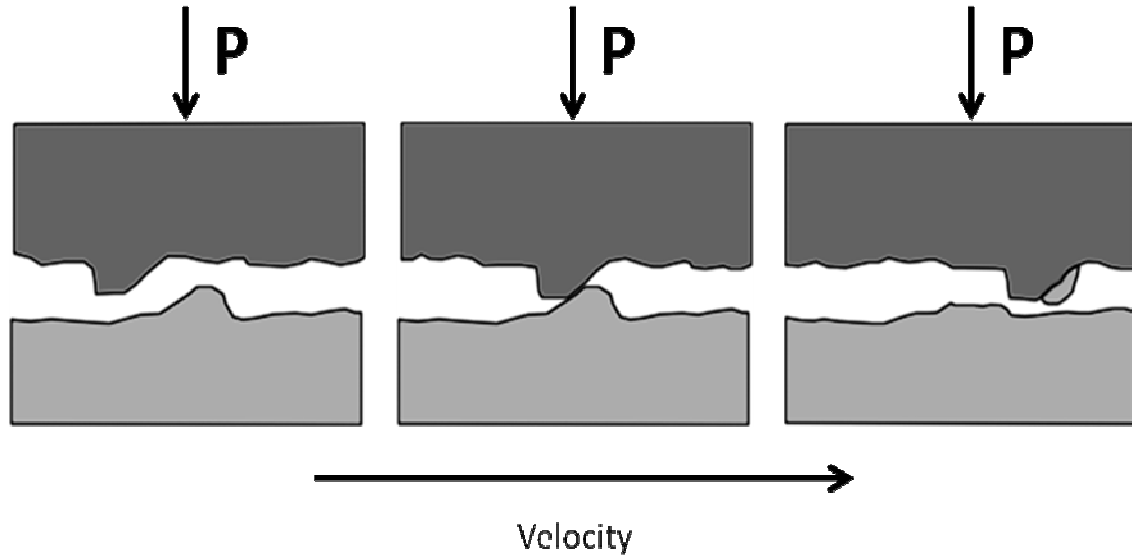
Figure 3. This figure illustrates the adhesive removal of one material by another.

Fretting is a type of corrosive wear that combines the effects of abrasive and adhesive wear. Essentially, fretting describes the destructive nature of corrosion based wear debris as it moves in between the two surfaces. When the wear debris undergoes a tribo-chemical reaction and oxidizes, for example, the oxides will cause damage to the surface since it is a much harder material. The Archard-Holm law is often used to model this type of wear [13].

Tribo-chemical reactions are those which occur as a result of tribological sliding between materials. Under a tribological setting, the materials undergo various chemical reactions due to environmental influences, which will create new compounds. One mechanism responsible is absorption [15], which can change surface characteristics and form thin layers of new materials. A primary cause of tribo-chemical wear is the presence of humidity in the system [16]. You et.al and Cuong et.al for example, describe

the effects of relative humidity on carbide based coating in sliding contact [17, 18]. The combination of increased frictional heat and the presence of water vapor will cause the development of oxides on the surface. Oxides, being a much harder compound, will be a significant influence on the wear process.

1.4. Lubrication

The addition of a film of material between two interacting surfaces with the purpose of reducing the effects of friction between them is referred to as lubrication. By adding a lubricant in between the moving surfaces, not only can the friction be reduced but the wear and thermal energy as well. In addition, lubricants can serve to remove wear particles from the surfaces thus improving the flow of motion and reducing the chances of those particles causing abrasive damage. A lubricant can be in the form of a liquid, solid, gas, or any combination thereof. The proper application and selection of a lubricant can significantly prolong the life of mechanical components. Essentially, there are three different modes of lubrication [19]: boundary, fluid film (hydrodynamic), and mixed lubrication (elastohydrodynamic). Figure 4 shows the different types of lubrication. In this figure, the darkened area is the lubricating layer. It has three major areas as shown.
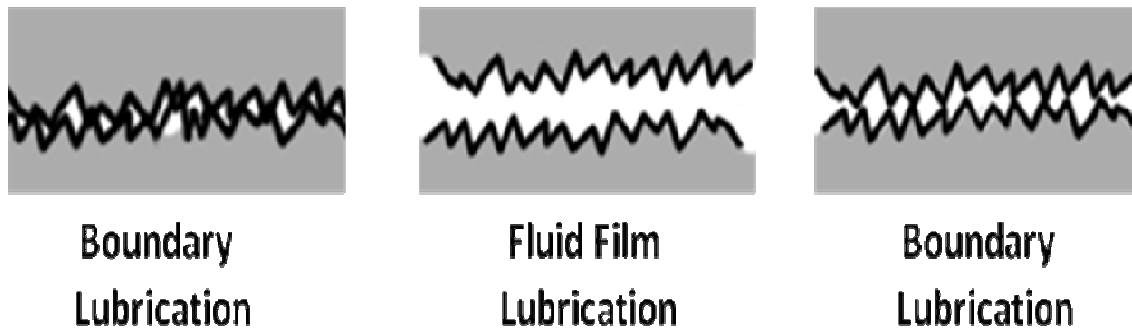
Figure 4. This figure illustrates the three different lubrication modes.

When a liquid lubricant is introduced between two moving surfaces, three distinct regimes of lubrication can be observed [20]. These regimes are illustrated in Figure 5 with the Stribeck Curve. The curve is typically used in the analysis of fluid bearings [21] and shows a relationship between the friction coefficient, f, and a dimensionless lubrication parameter called the Sommerfield Number. The Sommerfield Number, S, is represented by the following equation:

$$S = \left(\frac{r}{c}\right)^2 \frac{\mu N}{P} \tag{3}$$

Where r is the shat radius, c is the radial shaft clearance, μ is the fluid viscosity, N is the revolutions per minute (RPM) of the shaft, and P is the dispersed load on the bearing area.
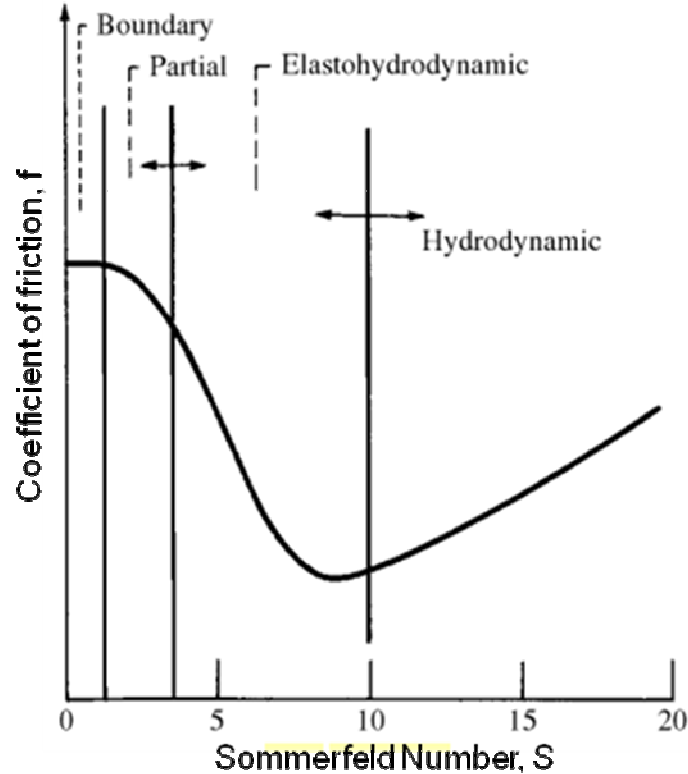
Figure 5. Typical Stribeck Curve [22].

As shown by the Stribeck Curve, the boundary lubrication regime has the highest friction coefficient. This shows that the applied load is carried by the surface roughness of the materials [23] as seen in Figure 5, and the lubricant has little to no effect. The friction will primarily be a function of the solid contact between the various surface characteristics.

The next regime in the Stribeck Curve represents mixed, or elastohydrodynamic lubrication. As the name suggests, the load will be carried by a mixture of both the surface roughness and the lubricant layer. Since the load will now be more supported by the lubricant, the friction will begin to decrease. As the Sommerfeld number increases

[24], less solid contact between the surfaces will occur, which will result in a much smaller friction coefficient.

At some critical point along the Stribeck Curve, the friction coefficient will begin to increase. In the hydrodynamic regime, the load will primarily be carried by the lubricant. The Sommerfeld Number will now be dominated by the viscosity of the lubricant [25]. The surface roughness will no longer play a role, and the friction will be dictated by the shear rate of the lubricant [22, 26].

1.5. Solid Lubrication

Solid lubricants differ from liquid lubricants in that they do not possess viscous properties. Typically, solid lubricants are used in situations where liquid lubricants would not be suitable to use [27]. These conditions can refer to high or low temperatures, high or low pressures, and high and low operating speeds. For purposes of this research, the extreme conditions will refer to high temperatures, and low pressures. The most common types of solid lubricants encompass four materials: graphite, molybdenum disulfide, polyfluoroethylene, and polytetrafluroethylene (PTFE) [28].

A solid lubricant is a dry material which reduces the frictional force between two contacting materials under relative motion. Different dry lubricants have different properties which attribute to their lubricating abilities. For materials such as graphite and molybdenum disulfide, the ability to provide a low friction environment is attributed to their lamellar, or layered, crystalline structure [22, 26]. Under working conditions, the layers will line up perpendicular to the direction of motion. The lamellar structures are held together by weak bonds, which provide low shear strength as the layers slide

against each other. Figure 6 illustrates the crystal structure of graphite, a common solid lubricant and a main focus of this thesis. Graphite and molybdenum disulfide based lubricants have a weak bonded layer as shown. During sliding, the layers slide against each other producing low friction. Details will be discussed in a later chapter.
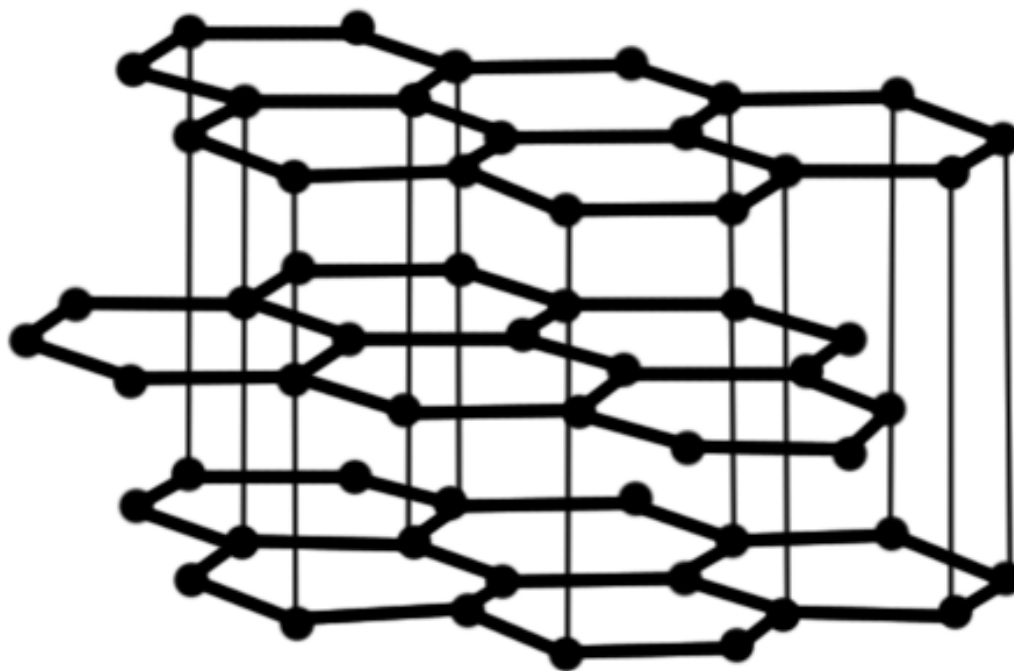
Figure 6. This figure illustrates the lamellar structure of graphite.

CHAPTER II

MOTIVATION AND OBJECTIVES

As discussed in Chapter I, lubricants have been used for centuries in countless applications. However, graphite based solid lubricants have been limited in their use in aviation and space travel types of equipment [29, 30]. The purpose of this thesis will be to evaluate the performance of graphite based coatings under the conditions they might experience when applied to aviation based turbo machinery. There is a need in aviation technology to implement carbon based coatings in bearing applications. The conditions to be examined will be high temperature, low humidity, and low pressure. The goal will be to determine whether the coatings will be acceptable for use in such applications as bearing in commercial airliner gas turbine engines.

The testing procedure will also be of significance in this research. The tribometer being used in the experiments has the capability of controlling the internal environment in terms of temperature, humidity, and pressure. Developing a procedure that best represents the actual working conditions of a particular coating will be critical.

The main objectives of this research will be the following:

1. Develop an understanding of the tribological properties of different coatings under extreme environmental conditions. Using a tribometer with high temperature and low pressure capabilities, carbon based and molybdenum disulfide coatings were evaluated.

2. Determine whether using carbon based solid lubricants will be acceptable for use in certain turbo machinery applications. Depending on the performance of the coatings, develop recommendations for improvements.

Overall, the findings in this thesis will be useful for the development of new coatings to be used in extreme conditions. The testing procedure will also be useful for evaluating other coatings that would undergo similar situations. This research will have relevance, not only for turbo machinery, but for any applications that require some form of lubrication.

CHAPTER III

MATERIALS AND METHODS

The purpose of this thesis is to evaluate the tribological characteristics of carbon based solid lubricants for applications in turbomachinery and other related fields. During normal operations, materials in turbomachines will experience wear during their lifetime due to several system factors. These factors will include, but are not limited to, the mechanical properties of the materials, the working load, rotational speed, and the environmental conditions. In order to effectively examine the wear mechanics of two particular materials against each other, an appropriate test must be chosen. In this thesis, the friction coefficient and the wear mechanisms of two materials in different combinations will be tested.

3.1. Tribometer

In order to measure the wear mechanics of the test samples, the apparatus used in this thesis will be a high temperature pin on disc tribometer. The pin-on-disc tribometer operates according to ASTM G99 standards [31]. The device consists of a rotating disc, and a stationary pin that is placed under a specified load. For purposes of this experiment, the pin will consist of a ball bearing. Figure 7 shows a basic diagram of the testing setup.
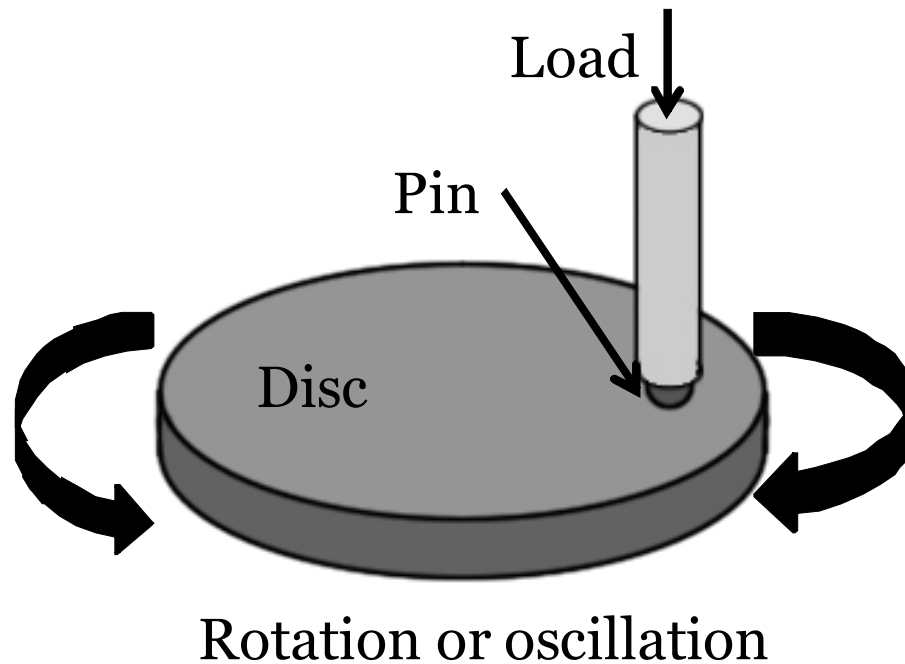
Figure 7. Testing configuration for a pin on disc tribometer.

During a given test, the disc sample is allowed to either rotate or oscillate. As the pin presses down onto the disc with some force, a circular wear track will be created. The pin is held in place by a solid shaft. The shaft is fitted with an array of load cells which measure its deflection as it travels along the disc sample. The change of the coefficient of friction between the disc and ball bearing will be determined by the deflection measured by the load cells.

As the test progresses, material will be lost from both test materials. The total wear rate for the disc and the pin will be determined from the amount of material that was lost during the course of the test.

The high temperature tribometer (HTT) used throughout this research is capable of collecting wear and friction data on test materials up to 1200°C. The furnace consists

of a reflective, gold insulating layer surrounded by electric heating elements. Both the

rotating platform and the shaft have just enough clearance to enter the chamber. When

engaged, the testing materials will essentially be enclosed within the furnace.

The entire apparatus is enclosed in a sealed glass bell jar. The bell jar allows for

the device to be evacuated for purging with dry gas and control of ambient testing

conditions. In addition, while the bell jar is engaged, the system can be placed under

vacuum pressure using a high vacuum pump. Figure 8 shows the overall system.

Figure 8. Image of the HTT used in these experiments, depicting the
heating element and glass bell jar.

The tribometer is equipped with a control console which handles all operations and displays data. The data from the tribometer is collected through a data acquisition card. The card is connected to a LabView® program which plots relevant information such as temperature, RPM, friction coefficient, and load.

3.2. Test Procedure and Conditions

The experiments for this research were conducted in such a way as to simulate working conditions for the coated samples. Each coated material, and ball bearing were set up in the tribometer in the same way.

First, the coated sample was placed on the rotating platform and secured. Each disc sample contained two blind holes 180 degrees apart, and a through hole in the center as seen in Figure 9. Each sample is two inches thick.
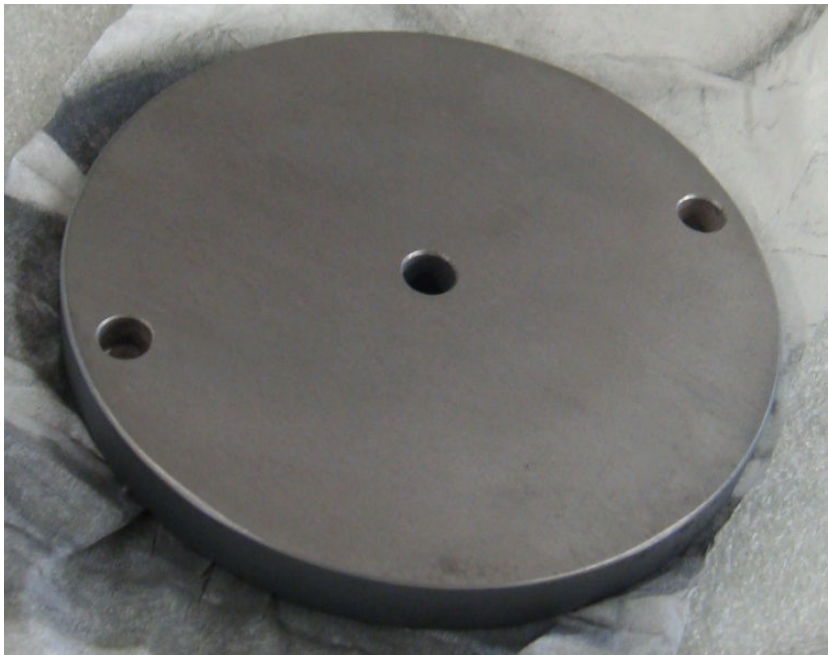
Figure 9. Bottom of the disc sample showing the thru and blind holes.

The HTT's rotating platform contains two pins which mate perfectly with the blind holes on the disc sample. When the sample is placed on the platform, a long bolt is then inserted to secure it in place, as seen in Figure 10.
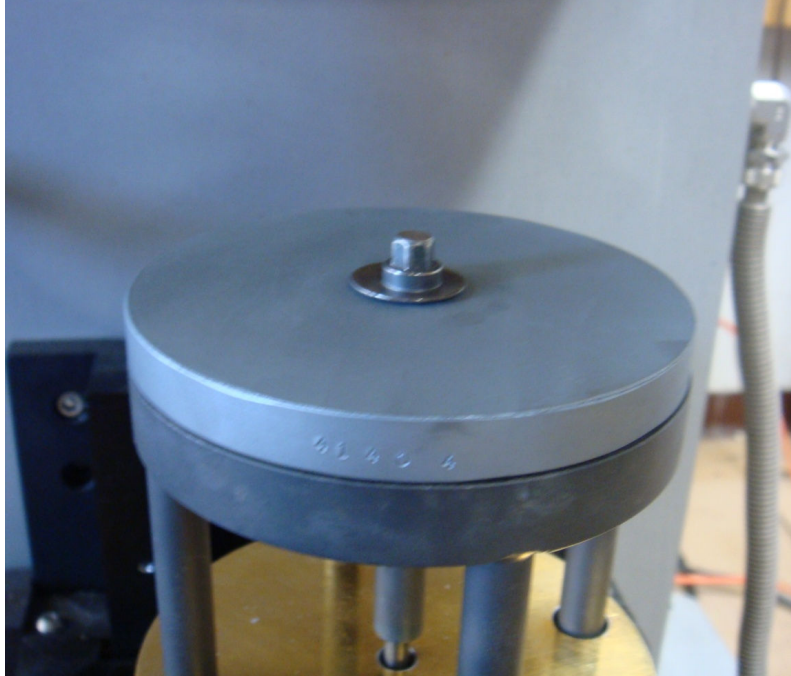
Figure 10. This figure shows the test sample secured to the rotating platform.

Once the sample was secured, the ball bearing was then placed into the shaft of the tribometer. The shaft is a solid stainless steel rod with a cup in which the bearing sits. The ball is secured by a large bolt, as seen in Figure 11. Prior to loading it into the machine, the ball bearing and shaft are rinsed with ethanol so as to remove any oil or contaminants that may have been transferred by the setup.

Figure 11. Ball bearing shown bolted in place on the load shaft.

The final sample assembly is shown in Figure 12. A test matrix was developed to establish all testing configurations for the experiments (Table 1). Atmospheric and room temperature tests were also conducted for comparison.

Table 1. Testing matrix

Disc Coating Material	Ball Material	Load [lbf]	Speed [osc/s]	Track Length [mm]	Relative Humidity [%]	Temperature [C]	Pressure [psig]
RGAC	440C	12	2.5	3	40	32	0
RGAC	440C	12	2.5	3	0	200	-12
RGAC	WC	12	2.5	3	40	32	0
RGAC	WC	12	2.5	3	0	200	-12
RGE	440C	12	2.5	3	40	32	0
RGE	440C	12	2.5	3	0	200	-12
RGE	WC	12	2.5	3	40	32	0
RGE	WC	12	2.5	3	0	200	-12

Each testing parameter involved a different procedure. The load for each test was up to 12 pounds.
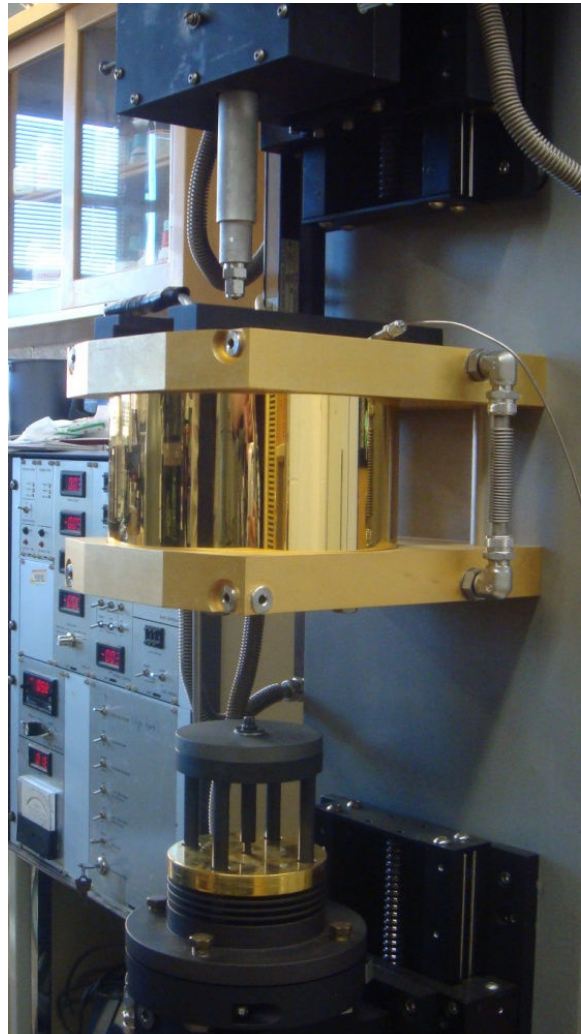
Figure 12. This figure shows the complete setup for the disc sample and
ball bearing.

For the atmospheric and room temperature conditions, the following procedure

was used:

1. The disc sample was raised into the heating chamber (which is turned off).

2. Next, the tribometer is set for a load of 12 pounds and the shaft is lowered onto

   the sample.

3. The tribometer is either set in oscillation or rotation mode, depending on the test.

4. The LabView® data acquisition software is started, followed by the tribometer motion.

5. The test is allowed to run for several minutes, as friction data is collected.

6. The test is ended and the sample and ball bearing removed.

The high temperature and vacuum tests are more complex and involve more steps. The purpose of these tests is to mimic working conditions for a turbo machine at high altitudes. At these conditions, the pressure is very low and there is virtually no humidity. Therefore, it is critical that the humidity in the chamber be continually monitored throughout the test. Humidity sensors are placed within the proximity of the heating chamber, and can be monitored visually through the glass bell jar. The sensors cannot withstand high temperatures, and are therefore placed as close to the heating chamber without causing damage. The following was the procedure used:

1. After the samples and ball bearing are loaded, the bell jar is lowered over the machine.

2. The sample is raised into the heating chamber.

3. The heating chamber is set to the desired temperature and turned on

4. The sample is allowed to sit inside the chamber for several minutes so as to reach a steady state temperature.

5. At the same time, the chamber is flushed with dry nitrogen gas so as to help reduce the ambient humidity.

6. The vacuum pump is turned on, and the pressure allowed to drop to -12 psig (for most tests).

7. The test will only proceed once the sensors read a relative humidity of below 2%. Since the sensors are not inside the heating chamber with the samples, it is assumed that the humidity inside the chamber is lower than that being read by the sensors.

8. The tribometer is set for a load of 12 pounds and the shaft is lowered onto the sample.

9. The LabView® software is started, followed by the tribometer motion (oscillation or rotation).

10. The test is allowed to run for several minutes as friction data is collected.

11. The test is ended and the materials are allowed to cool before they are removed from the tribometer.

3.3. Materials

The materials to be evaluated for this thesis were chosen based on their potential use in turbo machinery applications. In particular, they are intended to be used in bearings which frequently oscillate. However, their use is not strictly limited for this application. The solid lubricant coatings used in this research are a product of Everlube®. The coatings to be used will be the following:

1. Perma-Slik® RGAC

   This coating is a graphite based solid lubricant that provides a very low coefficient of friction. It remains stable at high temperatures, and works well in high loading applications. The samples used in this research were sprayed with a 0.3mm dry film coating. The dilution ratio is 1:1 product to solvent by volume.

The curing process included at least 6 hours at room temperature, with a relative humidity of 50%.

2. Perma-Slik® RGE-051

This coating is a lead free, inorganic, tungsten disulfide based solid film lubricant. It provides a low coefficient of friction, is stable in high temperatures, and performs well under high loading applications. The samples used in this research were sprayed with this coating for a dry film thickness of 0.3mm. The dilution ratio was 1:1 product to solvent by volume. The curing process included at least 6 hours at room temperature, with a relative humidity greater than 50%.

The following table shows the specifications of each coating:

Table 2. Design specifications as described by the manufacturer for each of the coatings [32, 33].

Coating	Lube Solid	Binder	Carrier	C.O.F	Max Temp. [^{o}C]	Load Capacity
RGAC	C	Organo-Metallic	Solvent	0.02-0.04	650	40K psi
RGE-051	MoS2	Organo-Metallic	Solvent	0.04-0.06	850	250K psi

The surfaces that the coatings will be tested against in the tribometer will be 6mm ball bearings made from the following materials:

1. 440C stainless steel (SS)

2. Tungsten carbide (WC)

The ball bearing materials, have the following properties shown in Table 3.

Table 3. Material properties for the ball bearing materials [22,34].

Material	Density [g/cc]	Hardness	Modulus of Elasticity [Gpa]	Tensile Strength [Mpa]	Poisson's ratio
WC	15.7	HRA 90	669	344	0.233
440C SS	7.8	HRB 97	215	1365	0.283

3.3.1 Carbon Based Coatings

Carbon based solid lubricants lend their lubricating properties to graphite. Graphite as a dry lubricant has been used for centuries [5]. It is an allotrope of carbon, consisting of a lamellar crystal structure, and low density. It occurs naturally and has the properties of both a metal and a non metal [35]. As seen in Figure 6, the crystal structure consists of layered hexagonal rings called graphenes. Each graphene structure is covalently bonded to the adjacent structures. The graphene layers are bonded parallel to one another by weak Van der Waal bonds.

Graphite is an effective lubricant due to the strength of the layered graphene rings and the weak forces separating them. As friction forces develop, the graphenes will line up parallel to the direction of motion. The weak Van der Waal bonds allow the layers to easily slide parallel to each other with very low shear strength. In the direction perpendicular to the motion, high compressive strength is offered by the layers. The sliding of the layers will effectively reduce the coefficient of friction between two moving materials [36].

As a lubricant, graphite is very effective. However, its lubricating effects are highly dependent on ambient water vapor. When water vapor is present, it gets absorbed into the crystal structure. The water interacts chemically with the graphite and causes a degradation of the bonds holding the graphene layers together [25]. This deterioration of the bonds will allow the graphene layers to more easily slide against each other. When water vapor is absent, the bonds are much stronger and limit the motion of the layers. Under moist conditions, graphite has been recorded to have friction coefficients as low as 0.05 [37]. Therefore, graphite is best suited for normal atmospheric conditions.

The material being evaluated in this thesis will be Perma-Slik® RGAC. It is a carbon based solid film lubricant with an organo-metallic binder system [32]. The test samples were prepared by spray depositing the coating for a thickness of 0.3 mm. The coated samples were then left to cure at room temperature for several hours. The coating is rated as having a very low friction coefficient, and performs well under heavy loading conditions.

3.3.2 Molybdenum Disulfide Based Coatings

Molybdenum Disulfide, like graphite, has a hexagonal lamellar crystal structure. It is commonly used as a dry lubricant and in some cases is more effective than graphite. Unlike graphite however, it does not occur naturally to be directly used as a lubricant. Molybdenum disulfide requires substantial refinement to meet the requirements to serve as a lubricant.

The crystal structure consists of a molybdenum layer sandwiched between two sulfur layers, as seen in Figure 13. Weak Van der Waal bonds, which lend to low shear strength in the parallel direction, are located in between the sulfur layers. However,

unlike graphite, water vapor is not required to reduce the bond strength in between the layers. This gives molybdenum disulfide an advantage when operating in low humidity environments. As a lubricant, it performs well under extreme operating conditions [12]. Dudder et al. studied the effects of environment and found that molybdenum disulfide based coatings out performed carbon based coatings in low humidity systems [38]. Kaur et al. performed similar tests conducted in this research with pelletized molybdenum disulfide and found that the material performed well under conditions of varying extremes [39].
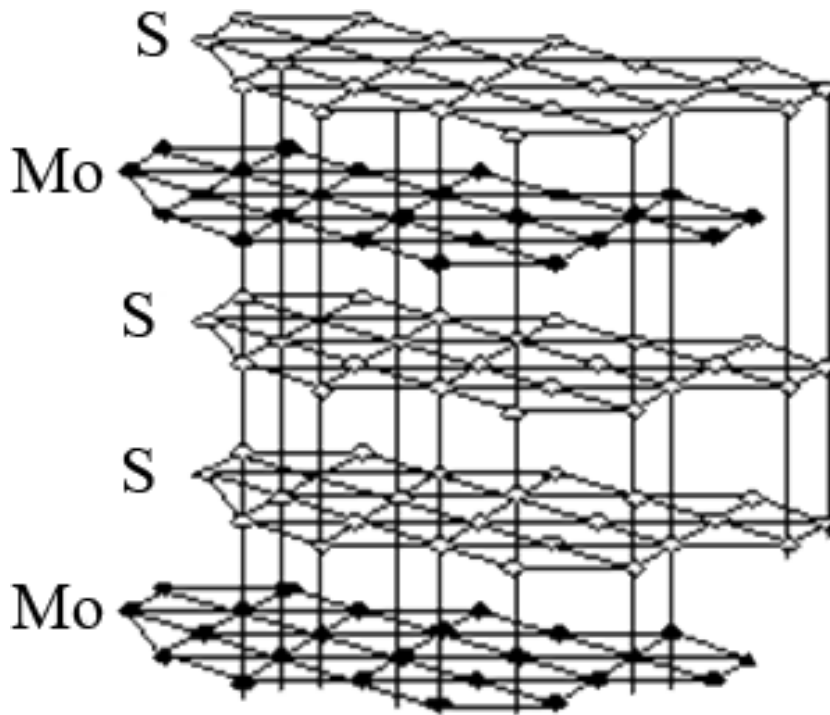
Figure 13. This figure illustrates the lamellar crystal structure of molybdenum disulfide.

The coatings that will also be evaluated in this thesis will be molybdenum disulfide based. The purpose of their evaluation will be to give a basis of comparison for

the carbon based coatings. The exact material being used will be Perma-Slik® RGE-051. It is a molybdenum disulfide based solid film lubricant with an epoxy binder system [33]. Similar to the previously mentioned material, the test samples were prepared by spray depositing the coating for a thickness of 0.3 mm. The coated samples were then left to cure at room temperature for twenty-four hours. The coating is rated as having a very low friction coefficient, good corrosion resistance, and performs best in high load carrying applications [33].

3.4 Wear Analysis

A wear analysis was performed on the samples to obtain a better understanding of the wear mechanisms for each material and test conditions. The wear on both the disc sample and the ball bearing were observed and analyzed.

3.4.1 Optical Microscopy

An optical microscope was used throughout the course of this research to both visually inspect the samples and to take measurements of wear morphology. The microscope used was a Keyence® VHX-600 Digital Optical Microscope, shown in Figure 14. This microscope uses a charge coupled device (CCD) camera to take high resolution images (54 mega pixels) up to 500 times magnification. The image is displayed on a 15 inch LCD monitor and can be measured in real time by using on screen utilities.

Figure 14. Keyence VHX-600 Digital Optical Microscope [40].

The optical microscope was used to analyze the wear characteristics of both the disc and ball bearing samples after testing. The wear track on the disc samples were analyzed and measured at 100 and 200 times magnification. The ball bearing wear scars were analyzed and measured at 200 times magnification.

3.4.2   Scanning Electron Microscopy

After tests were completed, the wear tracks of the disc samples were further analyzed using scanning electron microscopy. The microscope used was the Quanta 600 field emission scanning electron microscope (SEM). The field emission gun contains a Schottky emitter source. It also contains a fully controllable x-y-z stage wherein the samples were manipulated and positioned for imaging. Images of the wear track were taken at 1000 times magnification under high vacuum. The accelerator voltage for each scan was at 10kV and the focus range was 10.3 mm. The SEM is also capable of

performing energy dispersive spectrometry (EDS), which was utilized to determine the composition of the materials located in and outside of the wear track. The EDS analyses offered a preliminary analysis of the wear particles on the sample. A more in depth analysis was conducted using x-ray photoelectron spectroscopy (XPS).

3.4.3   X-Ray Photoelectron Spectroscopy

The wear debris generated from the friction tests were subjected to x-ray photoelectron spectroscopy analysis. For this analysis, the machine used was a Beamline 8.2 at Stanford Synchrotron Radiation Lightsource (SSRL). The machine uses near edge x-ray absorption spectroscopy at a range of 4000-17000eV. The goal of the analysis was to obtain a chemical composition any films that developed during the friction testing. The analysis was conducted only for the RGAC coating against 440C stainless steel at high temperature, low pressure, and low humidity. The primary reason for this is that molybdenum disulfide coatings have been extensively studied and the chemical composition of the wear debris is well known. In addition, since the disc sample substrate is made from tungsten carbide, having an analysis with the stainless steel ball bearing would yield more useful information than that of the tungsten carbide ball bearing.

3.4.4   Wear Track Profilometry

Once each test was completed, the amount of material that was removed from the disc sample due to the friction of sliding motion was measured and analyzed. The path in which the ball bearing travels on the disc sample is known as the wear track. The wear

track will contain material from the disc substrate, the solid lubricant film, and even

some material deposited by the ball bearing.

After each test was conducted, the wear tracks on the disc samples were analyzed

using a surface profilometer. The instrument used was the TR200 hand held surface

roughness tester, shown in Figure 15. The instrument uses a diamond tipped stylus to

measure the surface roughness of any given material. The device works by using sensors

which measure the change in inductance as the stylus is traced over a surface. An analog

to digital converter translates the inductance value to a surface depth value. The sample

is first placed on a level surface, then the stylus is used to trace over the wear area. The

stylus is traced along the length and width of the wear track to obtain an average depth

value. This value, along with the length and width dimensions obtained through optical

microscopy will be used to calculate the total wear volume.

Figure 15. TR200 surface roughness tester.

3.4.5   Wear Scar Measurement

The wear scar on each ball bearing was analyzed using an optical microscope at 200 times magnification. The dimensions of each scar were then measured using two-dimensional imaging software. An example of the measuring process can be seen in Figure 16. A three-dimensional analysis, such as that described by Blau and Jun [41] was not possible due to limitations in lab equipment. The scar was either of circular or elliptical shape; each involved a different method of analysis.

For simplicity, the wear volume was measuring using a two dimensional analysis. This method will not include any complex curvature of the scar or any pitting on the surface.

For a circular shaped scar, Equation 4 and Equation 5 [41, 42] were used to estimate the volume of worn material.

$$V = \frac{1}{3} \pi h^2 (3R - h) \tag{4}$$

$$h = R - \sqrt{\left(R^2 - \frac{D^2}{4} \right)} \tag{5}$$

Where V is the volume of material removed in cubic meters, R is the ball bearing radius, and D is the wear scar diameter.

The above equations are modified in order to calculate the wear on an elliptical scar. For an elliptical shaped scar, Equation 6 and Equation 7 [41, 42] were used to estimate the wear volume.

$$V = \frac{a}{3b} \pi h^2 (3R - h) \tag{6}$$

$$h = R - \sqrt{(R^2 - b^2)} \tag{7}$$

Where V is the volume of worn material in cubic meters, R is the radius of the ball bearing, and a and b are half the length of the long and short axis of the ellipse, respectively.
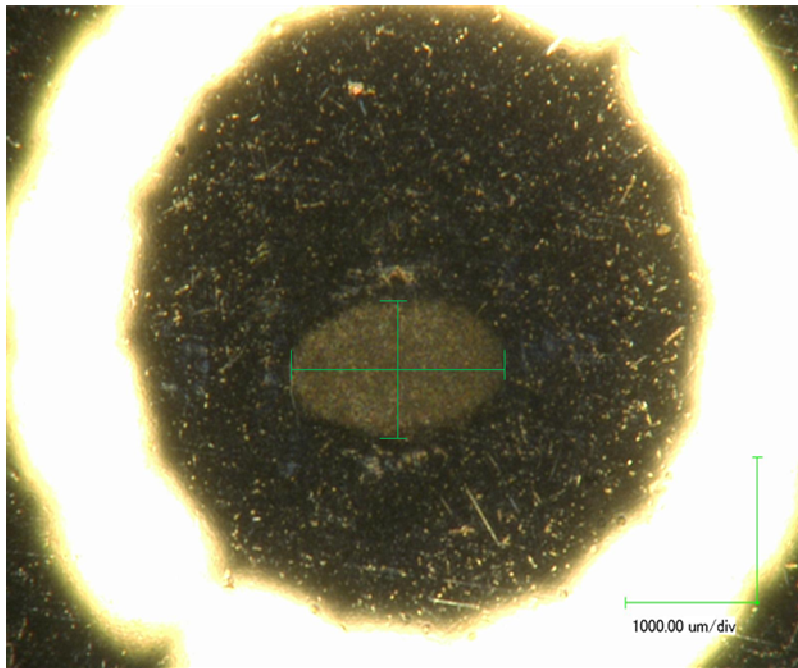
Figure 16. Optical microscope image of wear scar on 440C stainless steel ball bearing, showing measuring lines.

3.5 Hertzian Contact Analysis

The tribological experiments performed in this research involve a ball bearing coming into sliding contact with a flat disc specimen. When the two surfaces interact under static conditions, both elastic and plastic deformation will occur at their contact points [7]. The analysis being performed in this research will revolve around the Hertzian theory of contact. The assumption for each material in contact is that they are perfectly smooth and perfectly elastic [43]. As a result, the geometry of the contact area will be circular in shape. However, due to the concavity of the spherical ball bearing, the stress distribution will not be uniform. The center of the contact area will be under maximum compressive stress, while the outer perimeter will experience hoop, σ_h, and

radial, σ_r, stresses. A diagram of the contact surface and resulting stresses are shown in Figure 17.
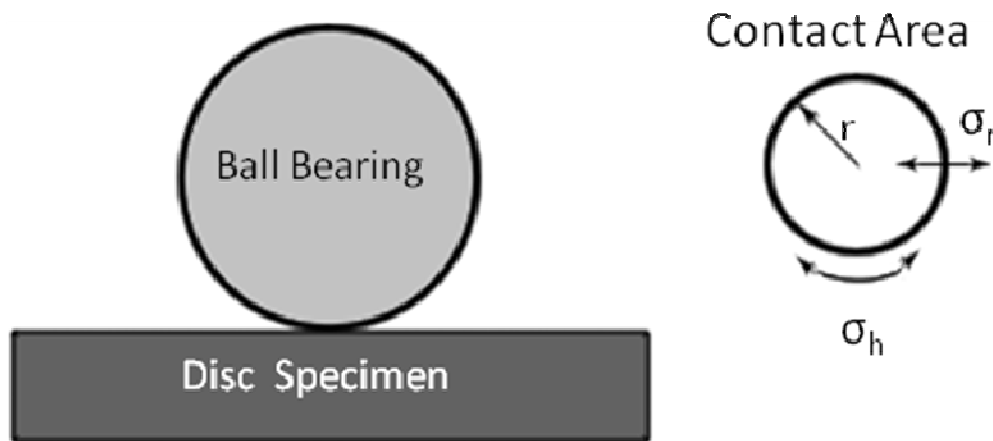
Figure 17. Diagram of the contacting surfaces, and Hertzian contact area with labeled stresses.

Since the hoop and radial stress have opposite magnitude, the perimeter will experience pure shear stress. Under static load, the maximum shear stress for this configuration will be located beneath the central point. The depth of maximum shear contact will be 48% of the total radius, r, of contact [35, 43].

The Hertzian analysis for static contact of the ball on flat disc model was performed using a series of equations as described by Jun and Truhan [44]. Since this analysis involves the interaction of two different materials of different geometry and mechanical properties, two relative relations need to be established (Mechanical properties of the materials are listed in Table 3 of section 3.3). The first is determining a relative radius for the materials. This was achieved using Equation 8.

$$R^* = \cfrac{1}{\left[\cfrac{1}{R_1} + \cfrac{1}{R_2}\right]} \qquad (8)$$

Where R_1 is the radius of the ball bearing, and R_2 is the radius of the disc sample. Since the disc sample is a plane surface, the value for R_2 will be zero. However, since we cannot divide 1 by 0, the effective radius will reduce to half the ball bearing radius. The next relation that must be established is a relative elastic modulus for both materials. This was done using Equation 9.

$$E^* = \cfrac{1}{\left[\cfrac{1-\upsilon_1^2}{R_1} - \cfrac{1-\upsilon_2^2}{R2}\right]} \qquad (9)$$

Where v_1 and v_2 represent the respective Poisson's ratio for each material, and R_1 and R_2 represent the radii of the materials. Again, since the disc material is a plane surface, R_2 will be equal to zero.

Now, the radius of the contact area can determined using Equation 10.

$$r = \sqrt{\left(\frac{3PR^*}{4E^*}\right)} \qquad (10)$$

Where r is the radius of the contact area, P is the applied load, R* is the relative radius of materials, and E* is the relative elastic modulus of the materials. The depth of contact, z, can be calculated from the radius using the following equation:

$$z = 0.48 * r \qquad (11)$$

The maximum Hertzian contact stress was calculated using Equation 12.

$$\sigma_H = \frac{3P}{2\pi r^2} \tag{12}$$

Where P is the applied load, and r is the radius of the contact area. From the maximum contact stress, the maximum shear stress can be obtained using the following equation:

$$\tau_m = 0.31 * \sigma_H \tag{13}$$

Table 4 lists the calculated Hertz contact values for the two combinations of materials. The disc samples are composed of tungsten carbide, while the ball bearings are either stainless steel or tungsten carbide.

Table 4. Calculated Hertz contact values for the material combinations.

Material 1	Material 2	R* [mm]	E* [Gpa]	r [mm]	z [mm]	σH [Gpa]	τm [Mpa]
SS	WC	1.5	351.4	0.09	0.043	3.28	1.0168
WC	WC	1.5	707.4	0.07	0.034	5.22	1.6182

3.6 Friction Measurement

During each test, LabView® software was used to collect data from the tribometer. The data included the temperature, the applied load, and frictional force. The primary means of characterizing the sample will be the coefficient of friction. As mentioned in Chapter I, the friction coefficient is the ratio of frictional force to the normal force. The LabView® software plots the change in friction coefficient over time as the test progresses. The data can then be collected and analyzed in Microsoft Excel. As a general rule, the coefficient of friction for a sample is measured at around 1000 seconds of a tribological experiment [35, 43]. This will give a good basis of comparison against different test samples. An example of a typical friction profile for an experiment is seen in Figure 18. The friction profile may have multiple peaks, which will vary depending on the material and the test conditions.
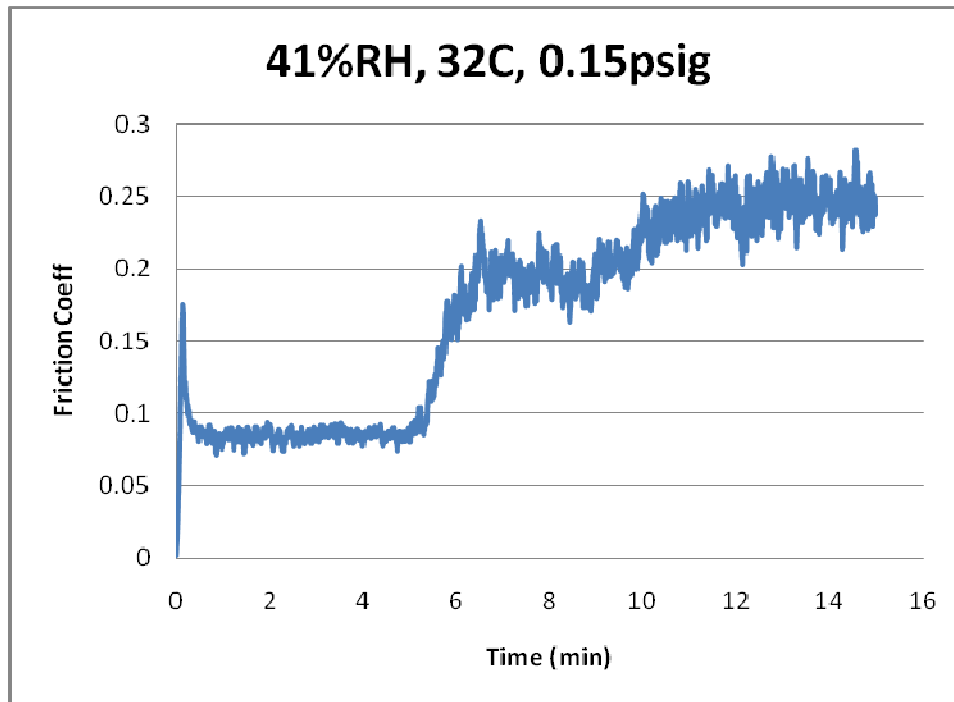
Figure 18. Plot of friction coefficient versus time for an RGAC sample against a stainless steel ball bearing.

In general, the friction profile will look similar to the one seen in the above figure. The friction may start off low, as seen in the figure, due to surface contaminations like absorbed moisture from the atmosphere. The low friction period may then increase sharply due to surface roughness [45]. Once surface roughness is removed, the friction will drop again. Next, the friction will enter a steady period in which it remains constant. For most experiments, there may only be one steady state region. However, due to the conditions described in Figure 18, the friction 'jumps' twice after a brief steady period. The increased friction coefficient will result from various wear mechanisms. These mechanisms may include abrasive and adhesive wear depositing debris into the wear surface, tribo-chemical reactions developing much harder oxide particles, or a combination of the three.

CHAPTER IV

RESULTS

After performing several tribo-testing experiments, the friction and wear mechanisms were analyzed through several methods, as described in Chapter III. The results showed that the performance of the carbon based coating greatly reduced when exposed to severe operating conditions. In comparison, the performance of the molybdenum disulfide based coating was comparable throughout all experiments.

4.1   Friction Analysis

The change in friction coefficient over time was measured during each experiment. After all experiments were completed, all of the friction versus time data were plotted and compared. A typical friction plot can be seen in Chapter III, Figure 18. Statistical analysis was performed to determine, if there was any difference among each of the tests.

First, the performance of the RGAC coating against the stainless steel ball bearing was analyzed. Figure 19 shows a typical friction response at atmospheric testing conditions. The figure clearly shows that the friction coefficient remains steady at around 0.25.
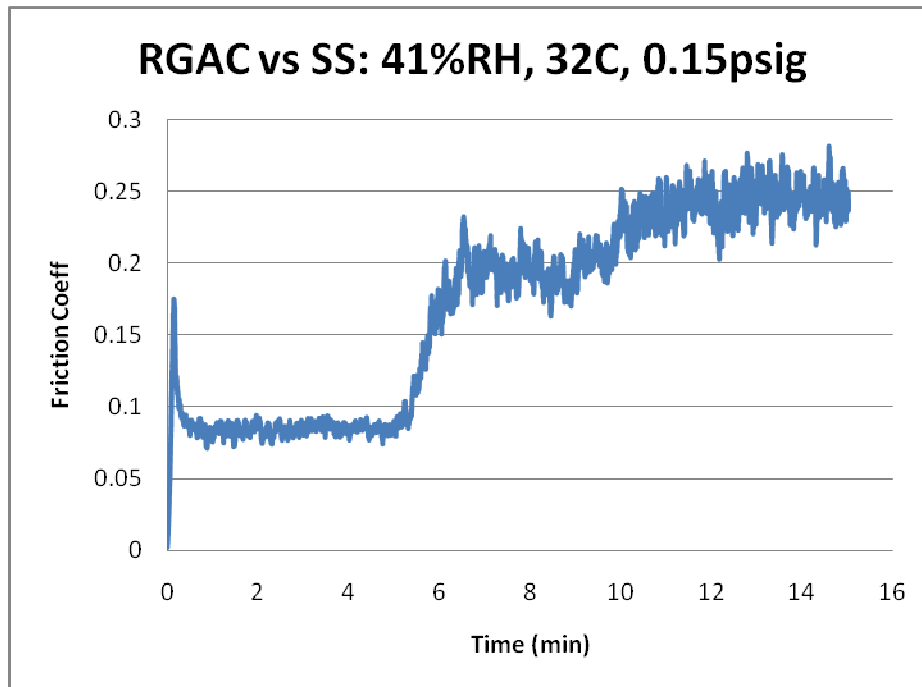
Figure 19. Friction response of the RGAC coating against SS, at high humidity, room temperature, and atmospheric pressure conditions.

In contrast, the same material pairing performed differently when tested under extreme operating conditions; high temperature, low humidity, and vacuum pressure. Figure 20 shows a typical friction plot. The plot clearly shows a significant increase in friction coefficient, reaching a steady value of about 0.4.
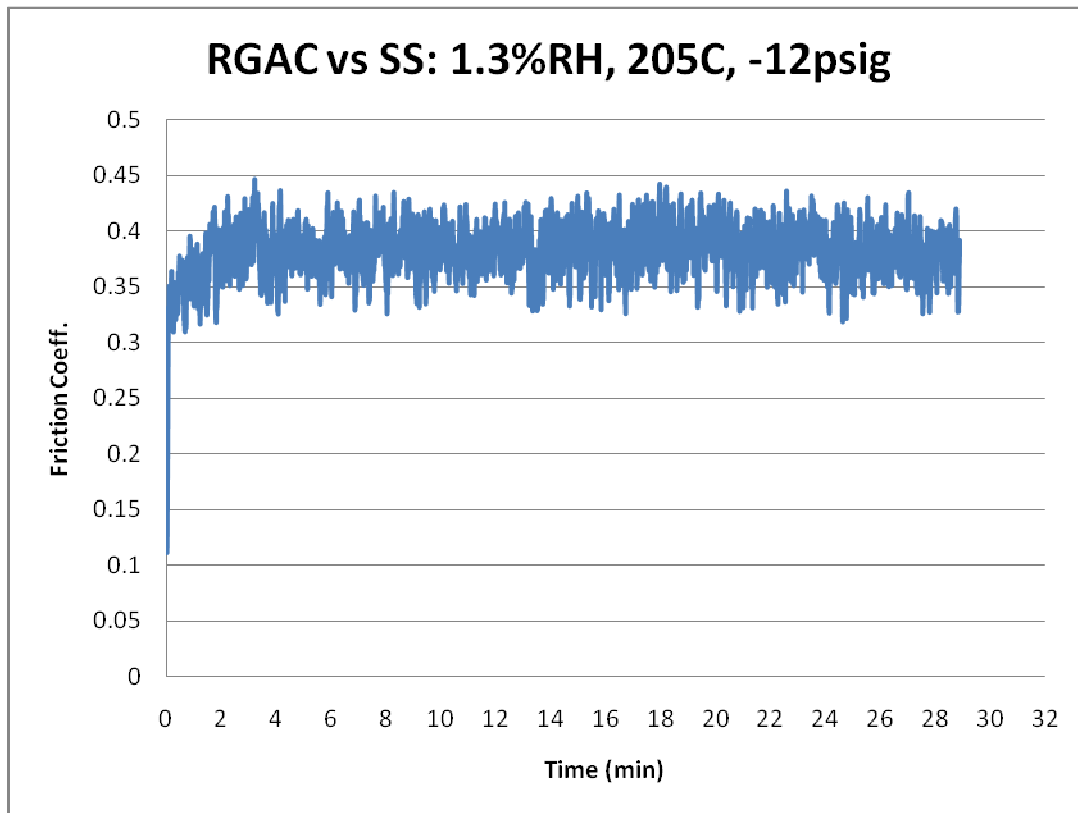
Figure 20. Friction response of the RGAC coating against SS, at low humidity, high temperature, and vacuum pressure conditions.

Several more tests were conducted and the steady friction values were collected after each test. Five tests were performed at atmospheric conditions and five at extreme conditions for RGAC against SS. A statistical comparison can be seen in Figure 21, with the RGAC, carbon based, coating against the stainless steel ball bearing material.
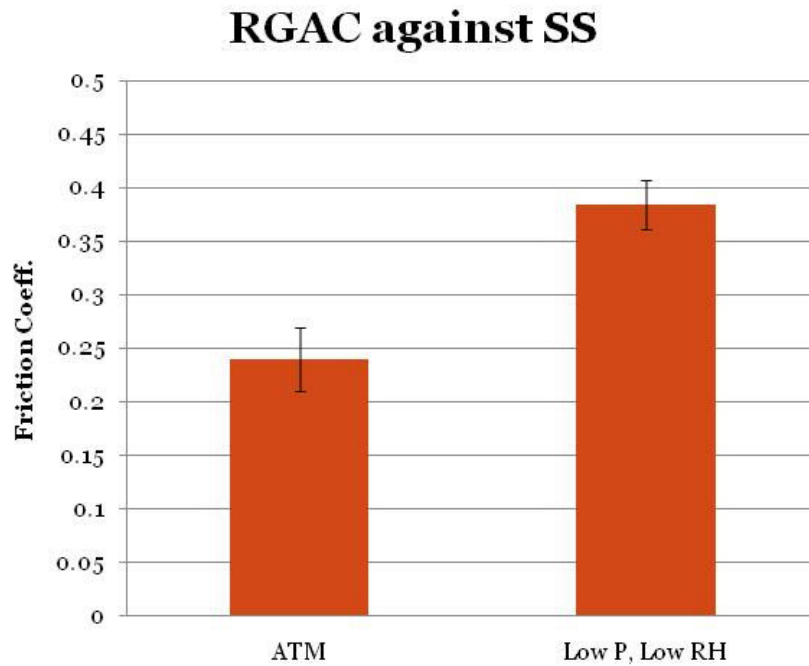
Figure 21. Friction coefficient for the RGAC coating against the 440C
stainless steel ball bearing at atmospheric and severe conditions.

The graph clearly shows that there is a significant performance difference in
coating material when performing under atmospheric conditions versus that in severe
conditions. Since this is the carbon based coating, initial analysis would show that the
friction increased due to the lack of ambient moisture.

Analysis continued with the RGAC coating against the tungsten carbide ball
bearing material. A typical friction response under atmospheric conditions is shown in
Figure 22. The plot clearly shows that the materials maintained a steady friction value
of less than 0.25, which is comparable to how the RGAC coating performed against SS
at the same conditions.
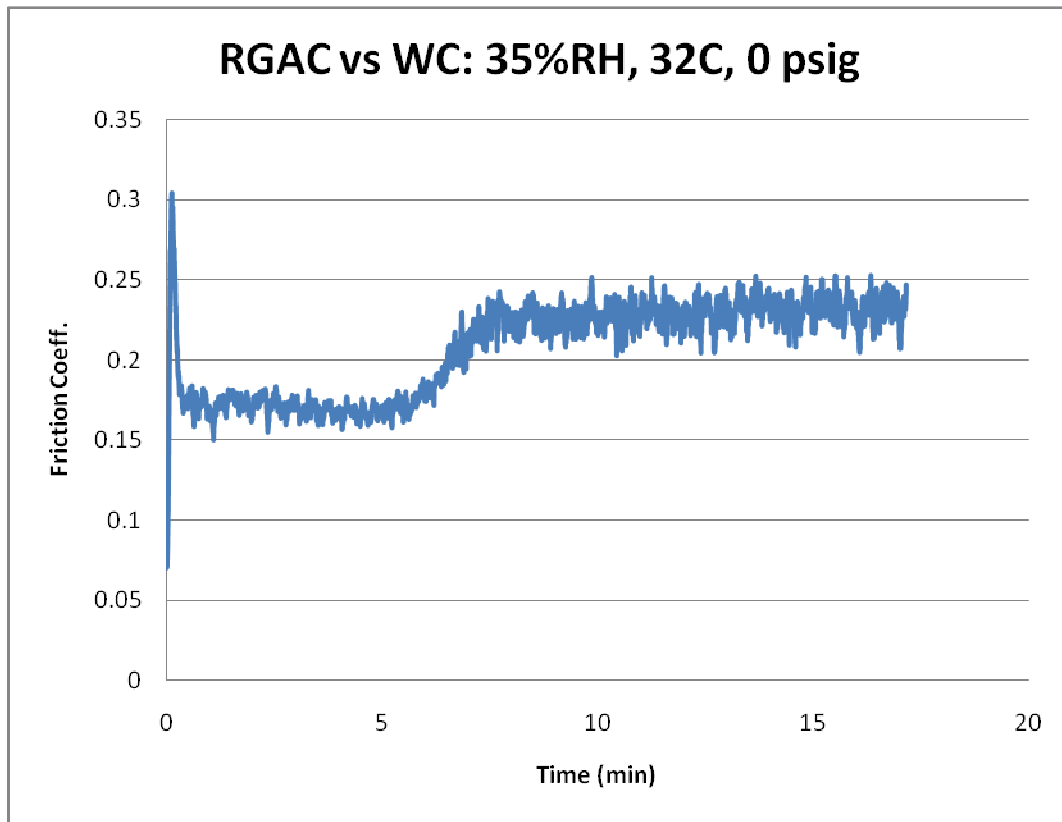
Figure 22. Friction response of the RGAC coating against WC, at high
humidity, room temperature, and atmospheric pressure conditions.

Again, the same material pairing performed differently when tested under

extreme operating conditions; high temperature, low humidity, and vacuum pressure.

Figure 23 shows a typical friction plot at the labeled test conditions. The plot clearly

shows a significant increase in friction coefficient, reaching a steady value of over 0.4.
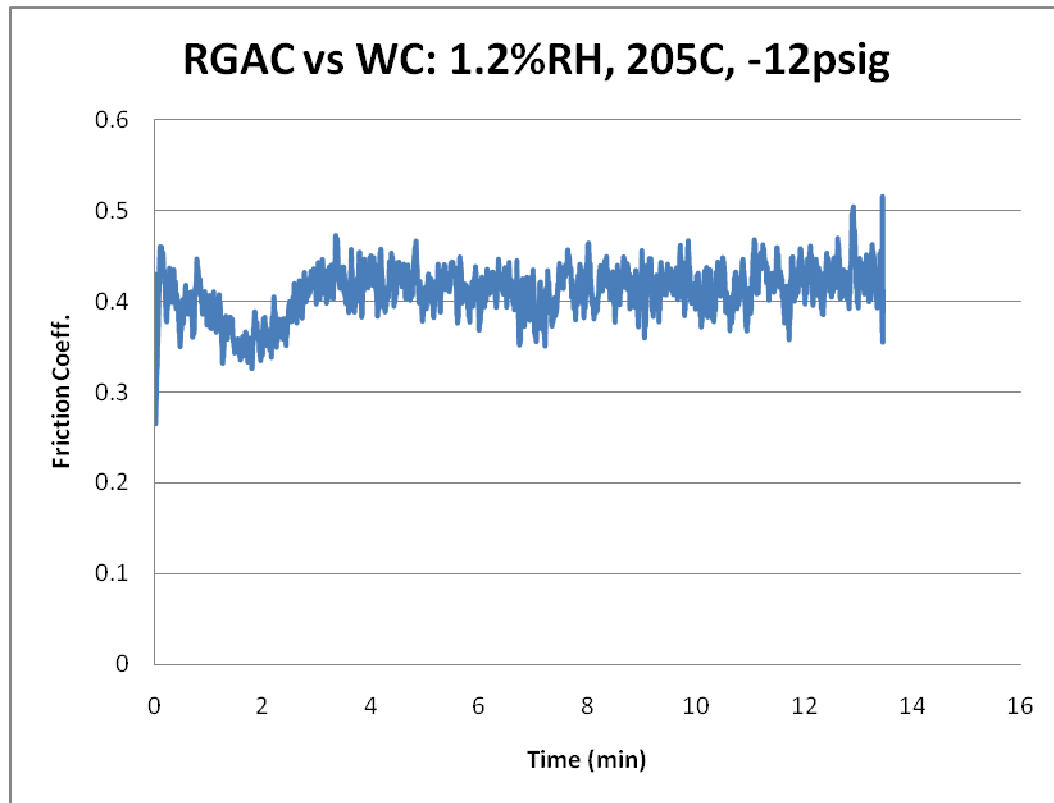
Figure 23. Friction response of the RGAC coating against WC, at low
humidity, high temperature, and vacuum pressure conditions.

Several more tests were conducted and the steady friction values were collected

after each test. Five tests were run at atmospheric conditions, while fifteen were

performed at extreme conditions for repeatability purposes. A statistical comparison can

be seen in Figure 24, with the RGAC, carbon based, coating against the stainless steel

ball bearing material. For the comparison, the number of samples was taken to be five to

obtain a more accurate comparison. However, the average value of the fifteen tests run at

extreme conditions was comparable to the five tests included in the statistical analysis.
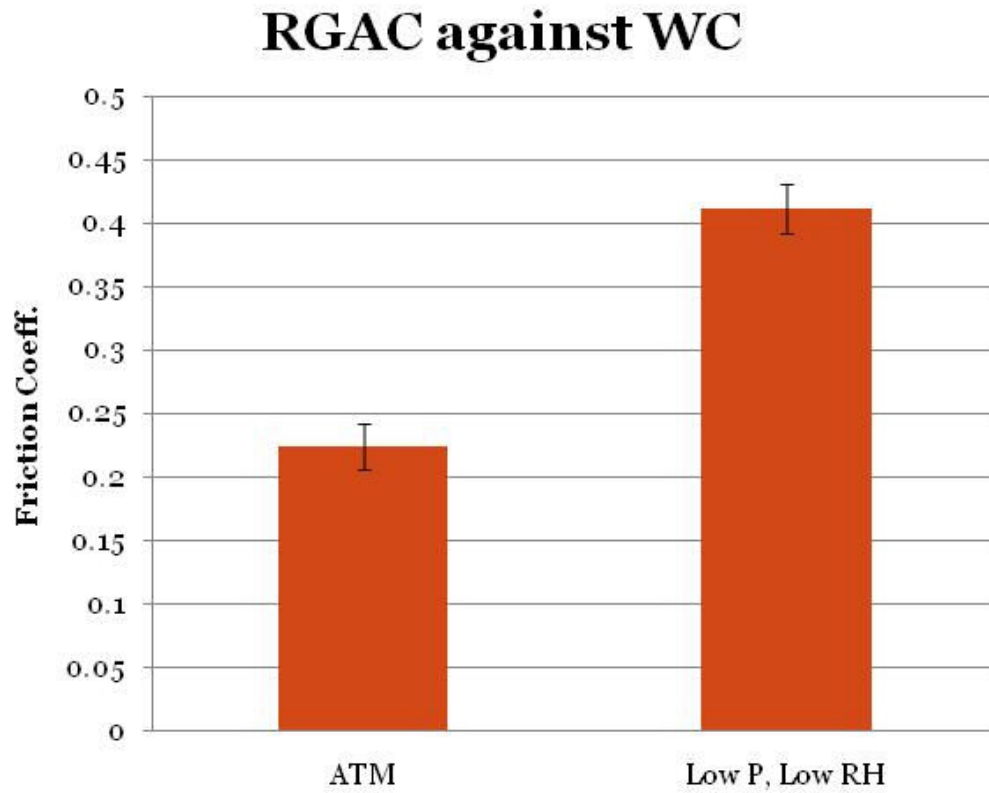
Figure 24. Friction coefficient for the RGAC coating against the tungsten carbide ball bearing at atmospheric and severe conditions.

Much like the previous results, this graph shows that there is a significant difference in friction performance when the RGAC coating is subjected to atmospheric conditions, versus those in severe conditions. Again, this is primarily the result of lack of moisture in the graphite structure.

The molybdenum disulfide based coating (RGE-051) was also analyzed for its performance against stainless steel and tungsten carbide ball bearings. Figure 25 shows a typical friction plot for RGE-051 against SS at atmospheric conditions. The plot clearly shows that the friction coefficient remained low at around 0.23
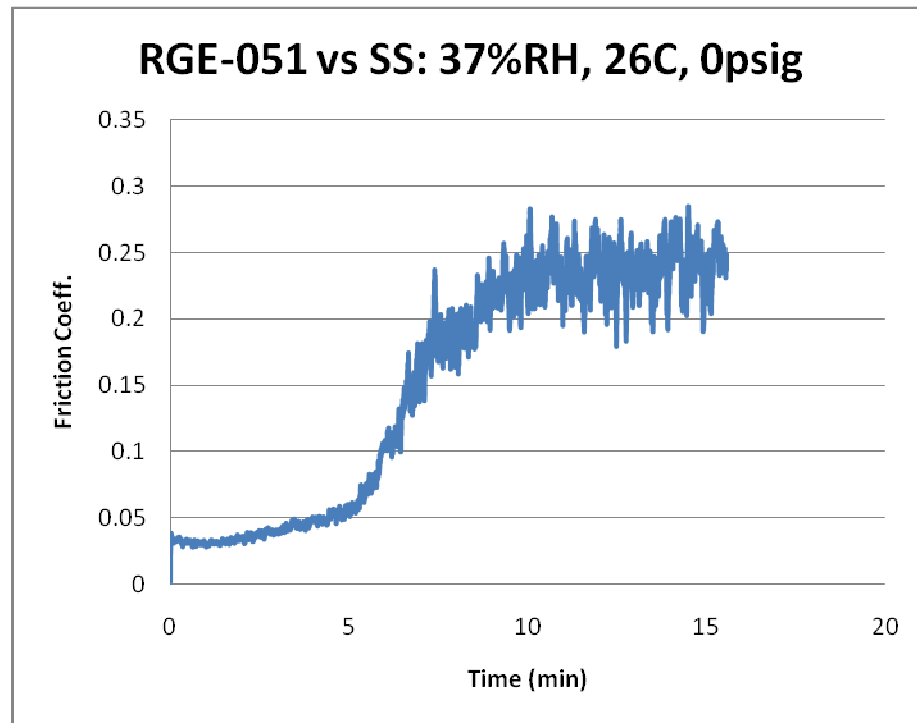
Figure 25. Friction response of the RGE-051 coating against SS, at high humidity, room temperature, and atmospheric pressure conditions.

Unlike the RGAC coating, the RGE-051 coating performed similarly at both atmospheric and extreme testing conditions. Figure 26 shows a typical friction response plot for the molybdenum disulfide based coating against stainless steel at high temperature, vacuum pressure, and low humidity. The plot clearly shows that the friction remains low at around 0.3, which is comparable to its performance at atmospheric conditions.
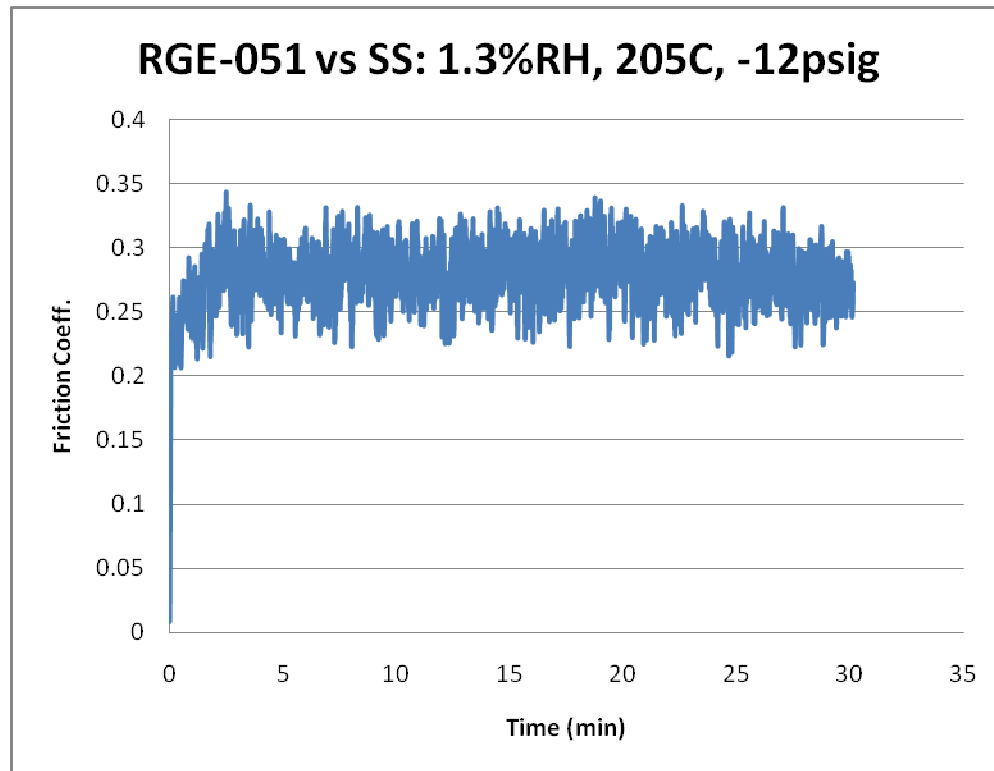
Figure 26. Friction response of the RGAC coating against SS, at low humidity, high temperature, and vacuum pressure conditions.

A statistical analysis was performed for the RGE-051 and SS material pairing. Since, the molybdenum disulfide coating is analyzed as a base comparison for the carbon based coating, fewer tests were performed. A sample size of three was used in the statistical comparison. The results of the comparison are shown in Figure 27.

Figure 27. Friction coefficient for the RGE-051 coating against the 440C stainless steel ball bearing at atmospheric and severe conditions.

Unlike the RGAC coating, the RGE-051 coating did not show a significant difference in friction coefficient when subjected to severe operating conditions. This is primarily due to the molybdenum disulfide structure not requiring moisture to create an effective lubricant. The high temperature, low pressure, and low humidity had little effect on the lubricating properties of this coating.

Further analysis was done on the RGE-051 coating against the tungsten carbide ball bearing. A typical friction response at atmospheric conditions is shown in Figure 28. Similar to its performance against SS at the same conditions, the coating maintained a low friction coefficient.
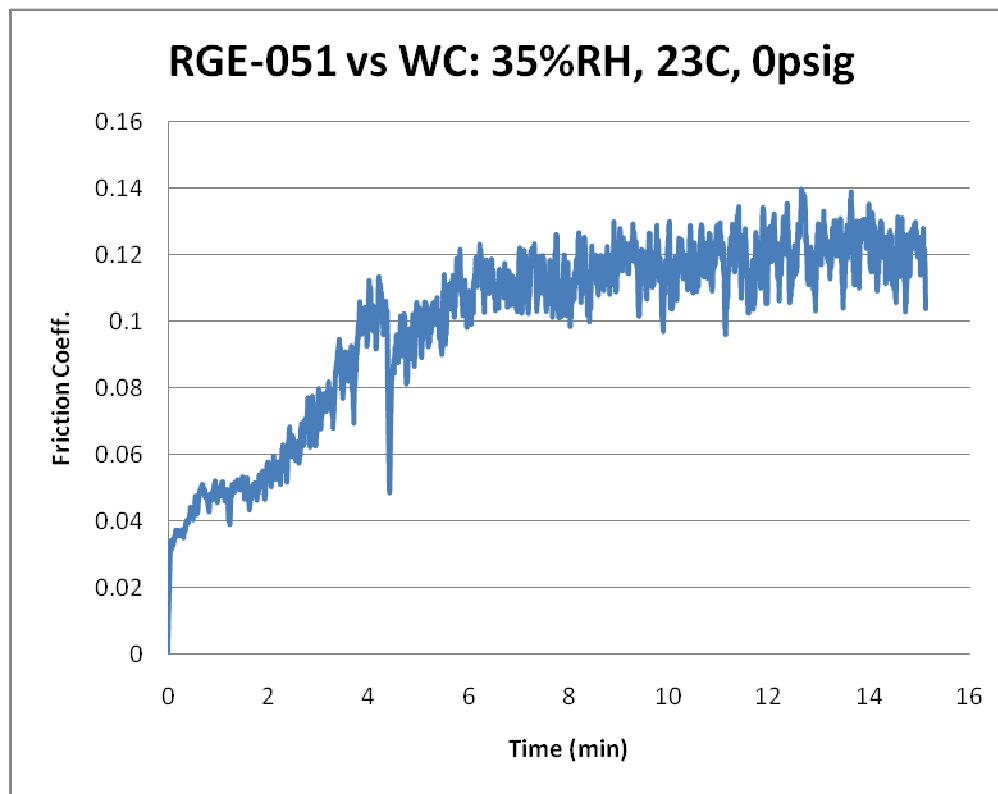
Figure 28. Friction response of the RGAC coating against WC, at high humidity, room temperature, and atmospheric pressure conditions.

The performance of the same material pair was also observed at extreme operating conditions. Figure 29 shows a typical friction response at high temperature, low humidity, and vacuum pressure. Again, unlike the RGAC coating, the RGE-051 coating performed similarly at these conditions. The plot shows that the friction remained low, much like response found in the plot in Figure 28.
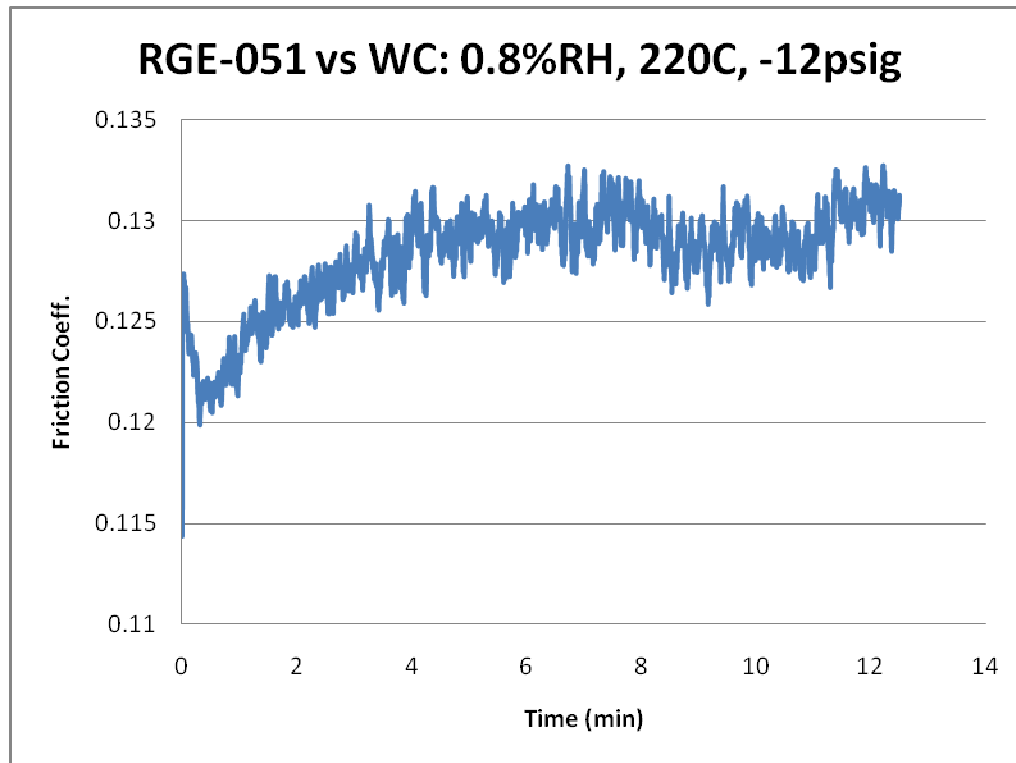
Figure 29. Friction response of the RGE-051 coating against WC, at low humidity, high temperature, and vacuum pressure conditions.

A statistical analysis was once again performed for the RGE-051 and WC material pairing. Again, since the molybdenum disulfide coating is analyzed as a base comparison for the carbon based coating, fewer tests were performed. A sample size of five was used in the statistical comparison. The results of the comparison are shown in Figure 30.
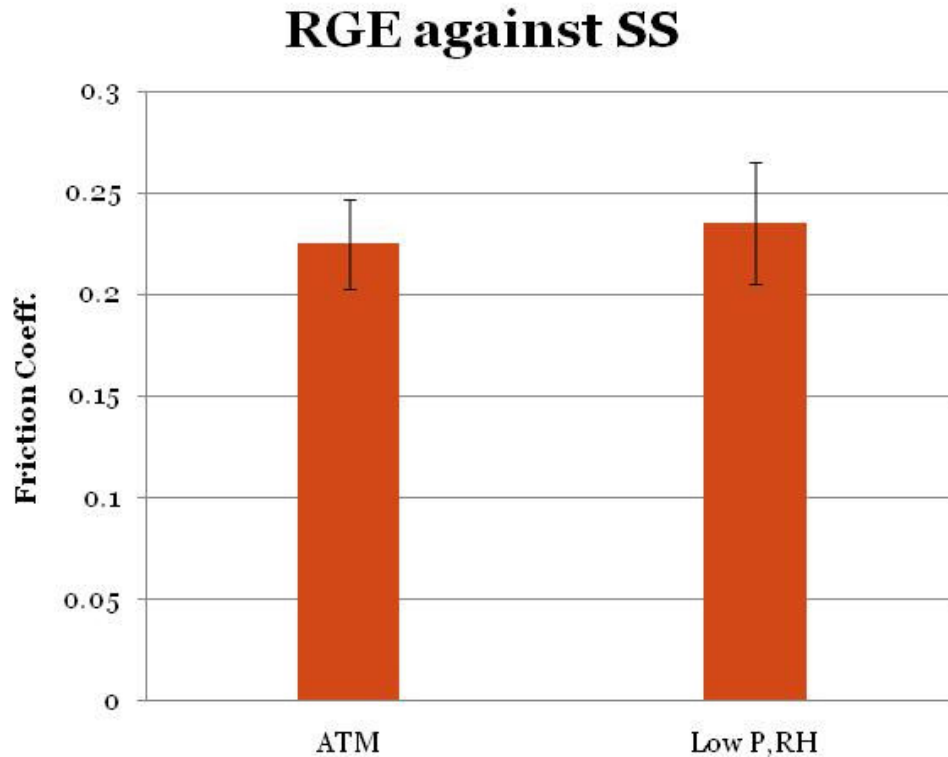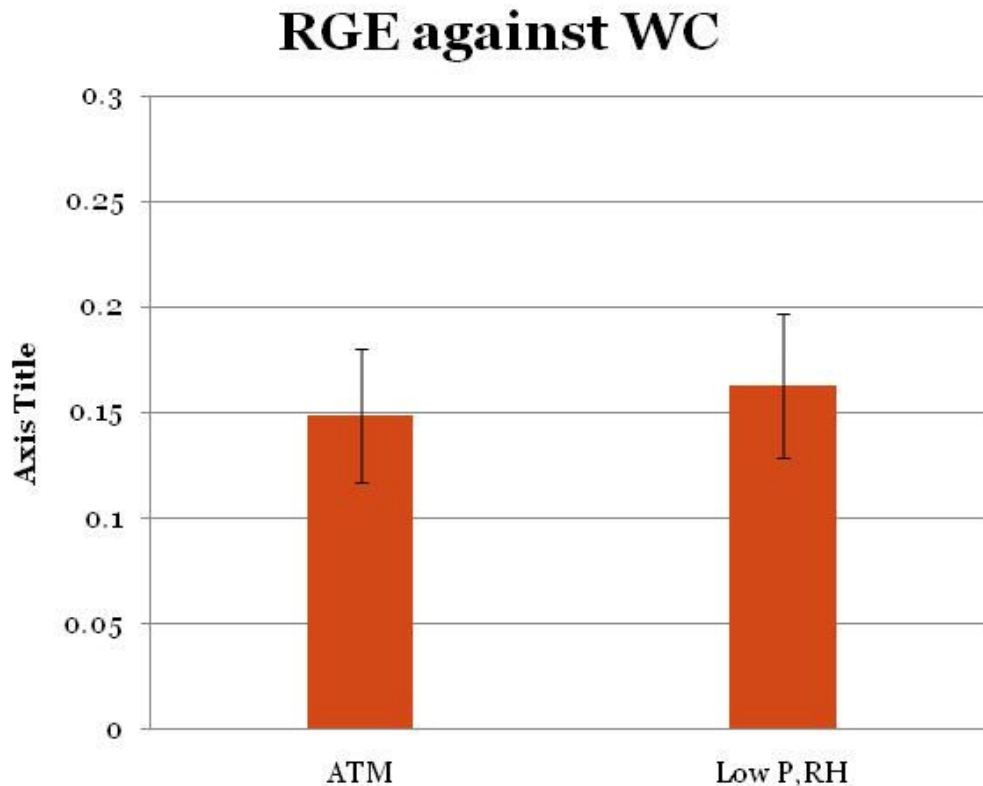
Figure 30. Friction coefficient for the RGE-051 coating against the tungsten carbide ball bearing at atmospheric and severe conditions.

Much like the previous result, the RGE-051 coating showed little difference in friction performance when subjected to atmospheric versus severe operating conditions. Again, this was due to the molybdenum disulfide structure not requiring ambient moisture to establish its lubricating effects.

Overall, the friction coefficient analysis showed that the carbon based lubricant performed poorly compared to the molybdenum disulfide based coating at severe operating conditions. Further analysis will be conducted on the wear tracks, the wear scars, and the wear debris to gain a better understanding of the mechanisms responsible for this difference.

4.2   Optical Microscopy Results

Once all the friction experiments were completed on a disc sample, they were subjected to analysis under an optical microscope. This analysis served to visually inspect the worn areas to better understand the wear mechanisms involved. The microscope was also used to measure the dimensions of the worn area in order to determine the worn volume, which will be discussed in section 4.3.

Figure 31 and Figure 32 show the wear tracks of the RGAC and RGE-051 coated disc samples when under atmospheric pressure, room temperature (32°C), and humid (40%RH) conditions. These images would correspond to the low coefficient of friction results discussed in the previous section.
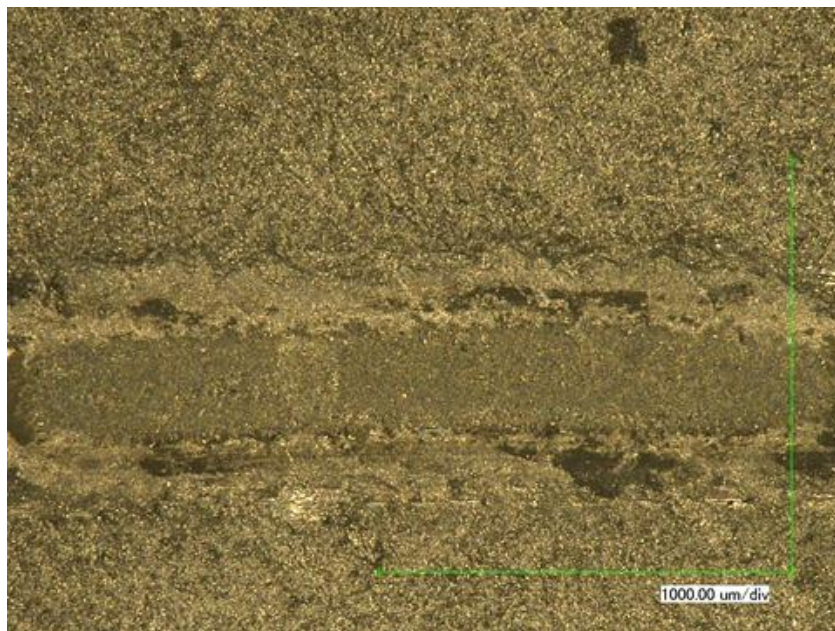
Figure 31. Optical microscope image of an RGAC coated disc sample that underwent atmospheric, humid test conditions.

The image in Figure 31 clearly shows a smooth film that developed within the wear track. This layer effectively formed a lubricant between the disc sample and the ball bearing, keeping the friction coefficient low. Also, there are little abrasive particles to be seen inside or along the edges of the wear track.
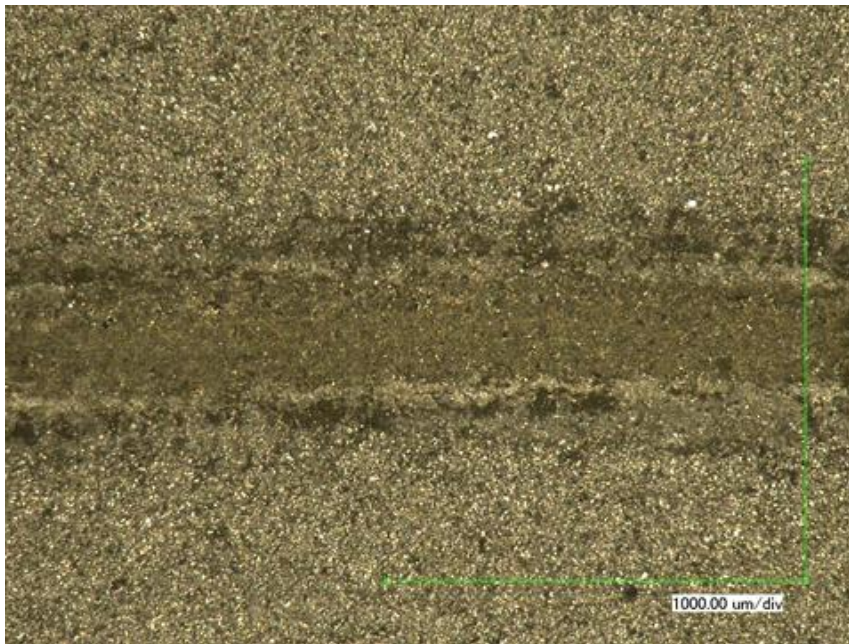
Figure 32. Optical microscope image of an RGE-051 coated disc sample that underwent atmospheric, humid test conditions against a stainless steel ball bearing.

Much like the previous figure, Figure 32 shows a smooth film within the wear track. This film formed an effective lubrication layer that helped to maintain a low coefficient of friction.

Figure 33 and Figure 34 show the wear tracks of the RGAC and RGE-051 coated disc samples when under vacuum pressure, high temperature (200°C), and dry (0%RH)

conditions. The RGAC image corresponds to the tests resulting in higher friction

coefficient.

Figure 33. Optical microscope image of an RGAC coated disc sample that
underwent vacuum pressure, low humidity, and high temperature
conditions.

Figure 33 clearly shows more wear along the outer edges of the wear track. This

abrasive wear mechanism is the result of wear debris, such as oxides, incorporating into

the wear area. The abrasive wear mechanism leads to an increase in friction coefficient.

When compared to the image in Figure 31, the inner wear track is much darker in color,

which indicates that the coating wore though and the substrate in more visible. This

wearing of the coating to expose the substrate will be will be further analyzed using

SEM and EDS, and discussed in a later section. The results seen in this figure will

correspond to the higher friction coefficients experience by this coating at extreme

conditions. A primary reason for the increase in friction is the absence of ambient water

vapor. The carbon based coating requires water vapor to degrade the bonds separating its lamellar crystal structure to form an effective lubricant.
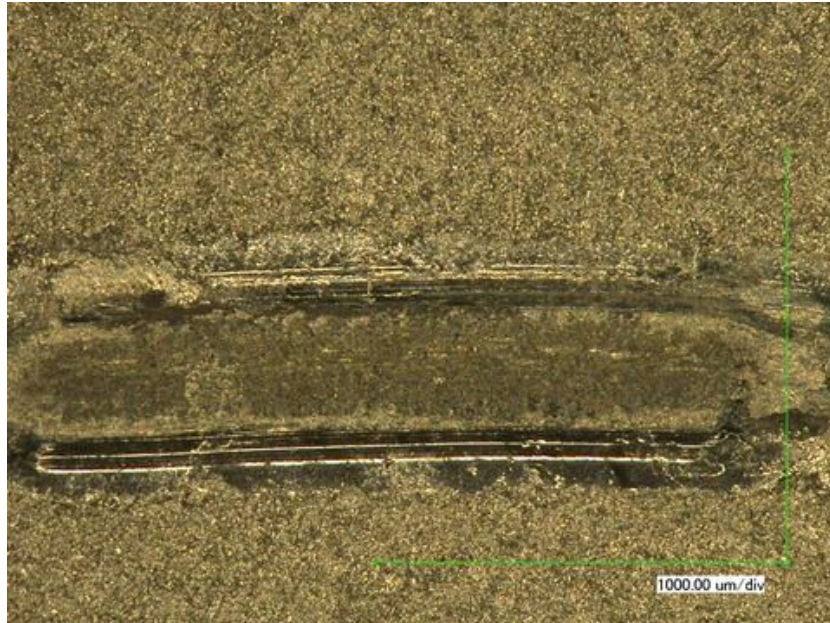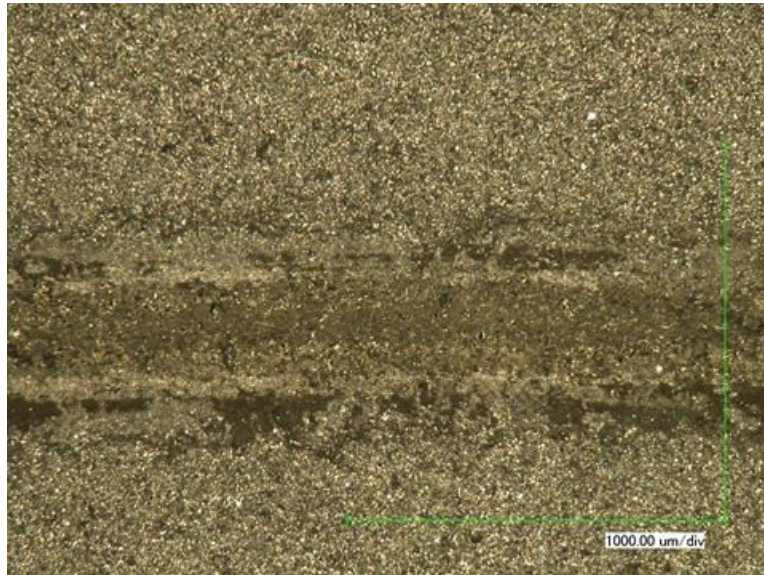

Figure 34. Optical microscope image of an RGE-051 coated disc sample that underwent vacuum pressure, low humidity, and high temperature conditions.

Unlike the results shown in the previous figure for a sample undergoing extreme testing conditions, Figure 34 shows no change when compared to the same sample undergoing atmospheric testing conditions. The RGE-051 coating performed as well in extreme conditions as it did in atmospheric conditions (Figure 32). As a result, the friction coefficient for both testing conditions was statistically similar, as discussed in the previous section. The result can be attributed to the molybdenum disulfide structure not requiring a humid environment to perform well as a lubricant [38].

4.3   Wear Volume Analysis

In addition to visually observing the worn areas on the samples, the wear volume was also measured using optical microscopy to gain better insight into the wear mechanisms for each material pair. As described in Chapter III, a two dimensional analysis was performed on each ball bearing using optical microscopy to determine the loss of material. In addition, a combination of optical microscopy and profilometry was used to determine the loss of material in the coated disc sample. The results for the wear volume are shown in Figure 35.
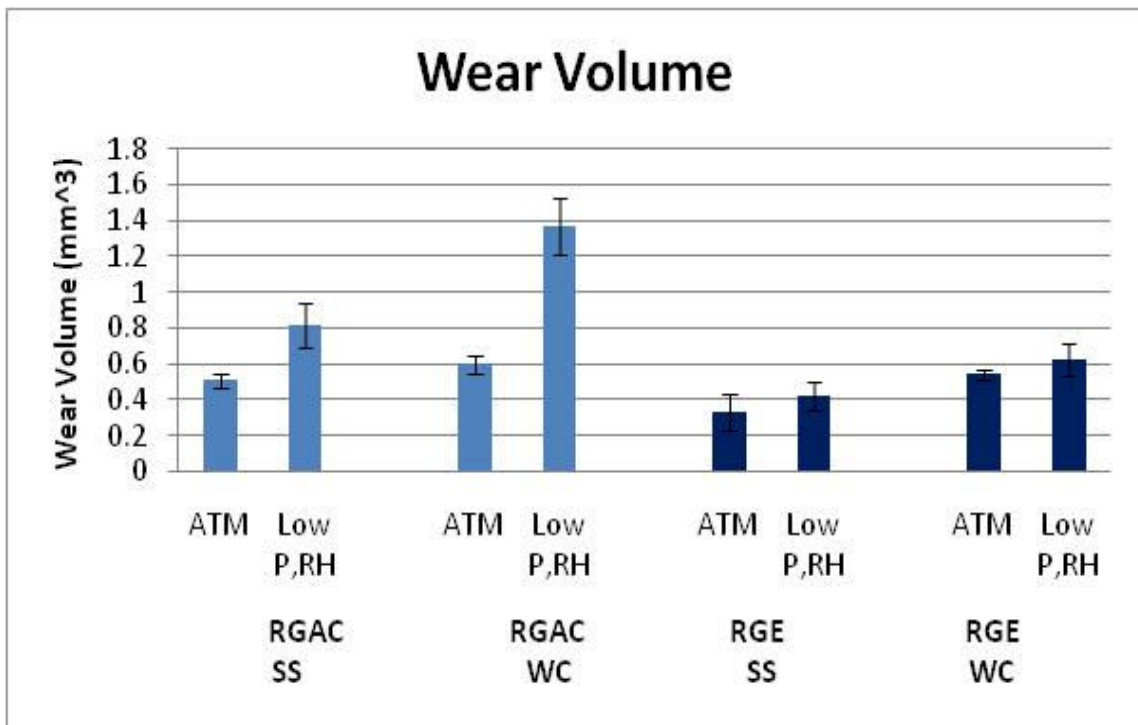
Figure 35. Measured wear volume for each material pair for the atmospheric and severe operating conditions.

As the graph shows, a greater amount of material was worn for the RGAC coating against the stainless steel and the tungsten carbide at severe conditions compared to atmospheric conditions. This is to be expected since the friction coefficient was much higher for these parameters. The molybdenum disulfide coating, however, remained statistically unchanged during each test.

From the wear volume results, it can already be shown that abrasion will be a dominant wear mechanism due to an increase in wear volume as the friction increases.

4.4   SEM and EDS Analysis

The wear track on the carbon based PermaSlik-RGAC coated disc samples were analyzed under a scanning electron microscope. The purpose of the analysis was to determine whether the coating was worn during the high friction experiments. Figure 36 and Figure 37 show the results of analyzing one set of parameters.
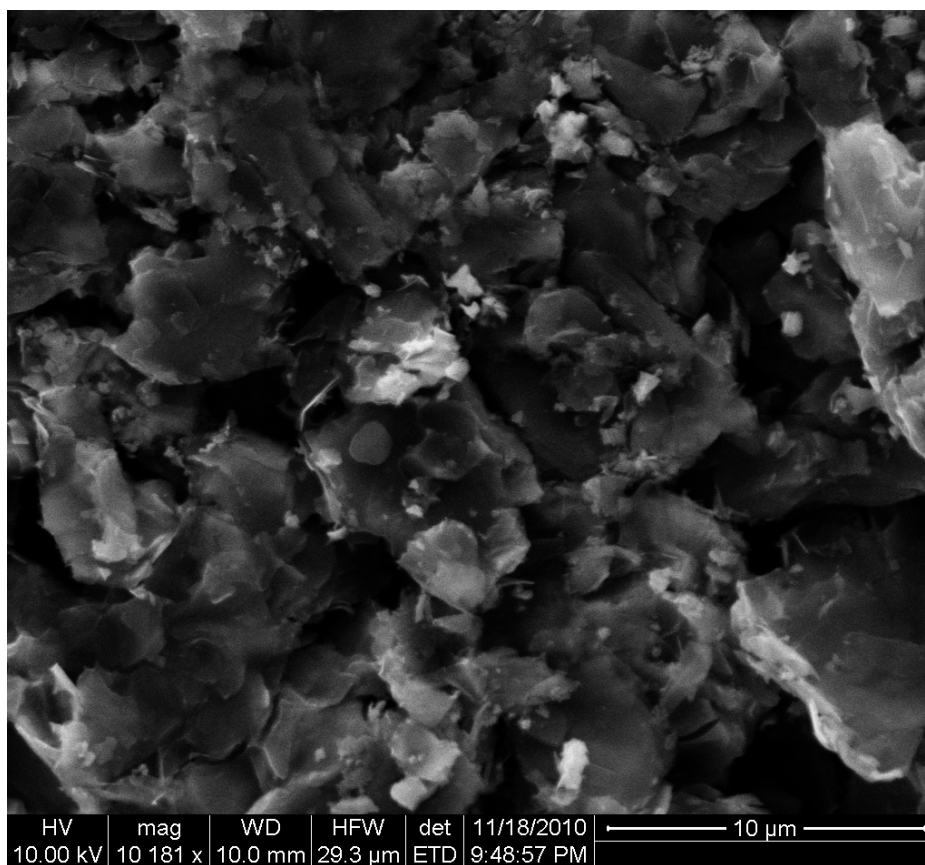
Figure 36. SEM image of the RGAC coating material.
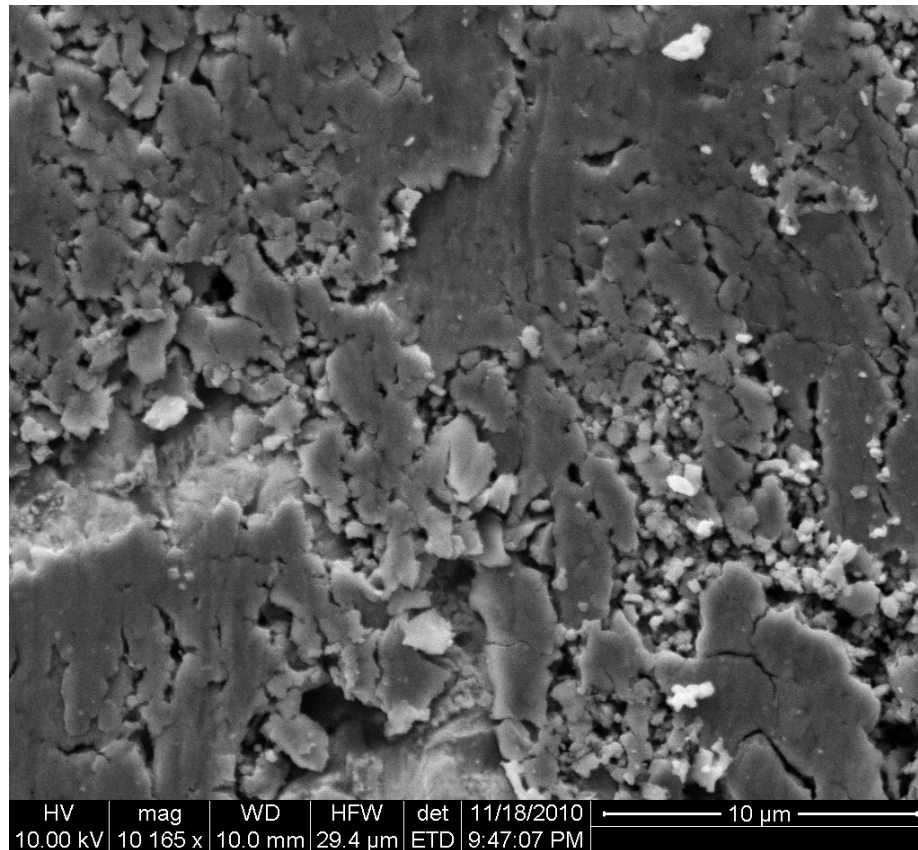
Figure 37. SEM image of high friction wear track on an RGAC coated
disc sample.

In addition to the SEM images, an Energy-dispersive X-ray spectroscopy (EDS)
analysis was also carried out on the samples. The same equipment was used in both
cases, as described in Chapter III. This process will yield a basis for comparison
between the elemental compositions of a coated portion of a disc sample versus the
interior of a wear track. This analysis was performed on a PermaSlik-RGAC coated disc
sample after undergoing a high temperature, low pressure, and low humidity friction
experiment. First, EDS was performed on a portion of the disc sample that was not
subjected to friction and wear. Figure 37 shows the resulting spectrum. Next, EDS was

performed on the center of a high friction wear track. The resulting spectrum for this

analysis can be seen in Figure 38.
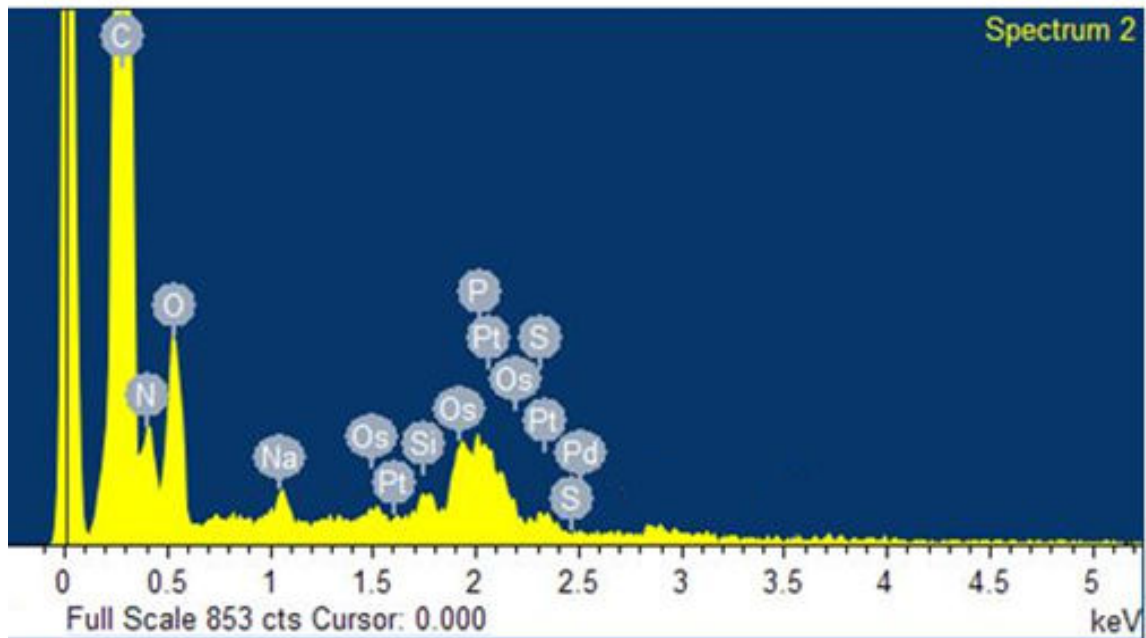
Figure 38. EDS spectrum of the elemental composition of the coated
portion of the RGAC disc sample.

As seen in Figure 38, the prominent element is carbon which indicates that the

sample is coated with a carbon based material. Other elements are present in the

spectrum as well. The oxygen may indicate some oxide formation on the surface, as

observed by Bregliozzi et al. [46]. However, since nitrogen is also present with oxygen,

this indicates that a mixture of air has been absorbed into the lubricant layer, as indicated

by Konca et al. [47]. The samples were exposed to air for long periods of time, and the

addition of extreme heat will further cause the absorption of air molecules into the

surface [27]. The figure also shows several more elements in the spectrum, such as

sodium, platinum, phosphorus, sulfur, and osmium. The sodium is representative of the

organometallic binder [32] that is used by the lubricant to adhere itself to the metallic

substrate. The remaining compounds appear to be randomly dispersed at the end of the

spectrum and may indicate some errors in the system, or some foreign contaminants

accumulated onto the surface as described by Mendez et al. [48] and Tsujikawa et al.

[49].
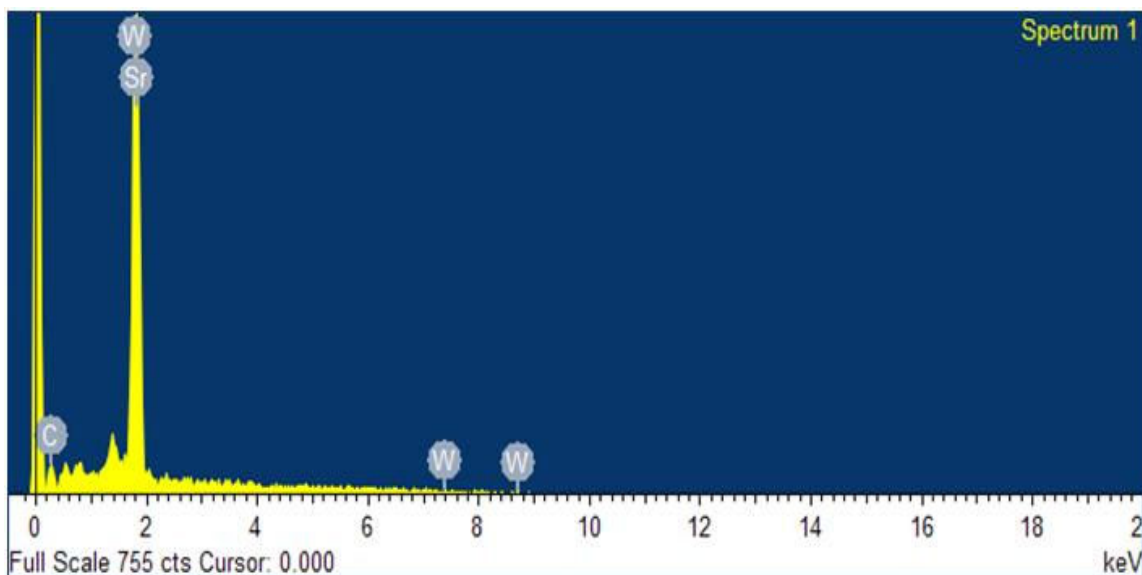
Figure 39. EDS spectrum of the elemental composition of interior of the
wear track on an RGAC coated disc sample.

As seen in Figure 39, the prominent elements are carbon and tungsten. When the

samples were analyzed, the wear debris had already been removed from the wear track,

so no additional elements from the lubricant will be present. Compared to the previous

analysis in Figure 38, this spectrum clearly indicates a difference in composition of the

different areas of the disc sample. Since the spectrum shows elements of carbon and

tungsten, this indicates that the coating was worn through to the tungsten carbide substrate of the disc sample. The spectrum also shows the element strontium as being part of the composition. Since it is located at the same peak as a tungsten element, it would indicate that the higher energy level of tungsten overlapped a lower energy level of strontium. Due to limitations in the EDS analysis in distinguishing similar energy levels [50], overlapping peaks will occur.

The combination of SEM and EDS analysis clearly showed that the lubricant coating wore away during a high friction tribological experiment. This will be an indication that the lubricant will no longer be serving its purpose and result in higher friction. However, other factors contributed to the change in friction and will be elaborated more in the next section.

4.5   Tribochemical Analysis

To gain a better understanding of the wear mechanisms responsible for the friction results, a tribochemical analysis was conducted. This analysis was performed using x-ray photoelectron spectroscopy, as discussed in Chapter III. The goal is to identify any and all elemental compounds present within the wear debris after a tribo-test was conducted. However, due to limitations in equipment, the XPS analysis was only conducted for one set of parameters: RGAC against 440C stainless steel at high temperature, low pressure, and low humidity. The results of the analysis were then analyzed to observe the elemental peaks that were present (Figure 40).
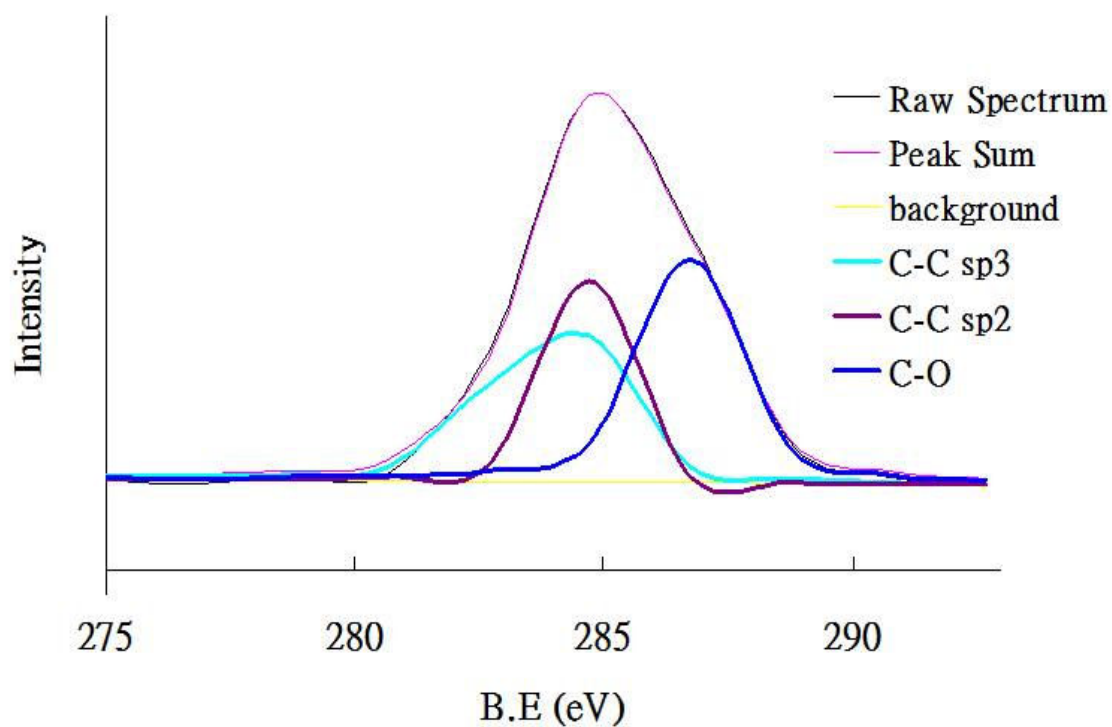
Figure 40. Results of the XPS analysis, showing the elemental peaks present in the wear debris.

The analysis showed that three distinct compounds were present in the wear debris after the tribo-test at extreme conditions. The first was C-C sp3, which is diamond like carbon. The second was C-C sp2, which is graphite. And the final was C-O, an oxide formation. A summary of the findings is located in Table 5.

Table 5. Specific data points associated with the various peaks found through XPS analysis.

Peak	Position [eV]	Area	FWHM [eV]	%GL
C-C sp3	283.804	0.756	0.790	80
C-C sp2	284.304	0.291	0.690	80
C-O	286.704	0.397	2.000	80

Diamond like carbon is an excellent tribology material due to its properties. It is able to resist abrasive and adhesive wear. The oxides, however, are a much harder material which can contribute to three body abrasive wear [51]. This abrasive wear, will be responsible for the increase in friction coefficient.

As mentioned before, the XPS analysis was only conducted on the wear debris for one set of parameters. This parameter was chosen because the main focus of this research is to determine how well the RGAC, carbon based coating, performs at extreme conditions. In addition, the stainless steel ball bearing was selected due to the nature of an XPS analysis [52]. Tungsten carbide is a more inert material than stainless steel [52], and since the goal is to analyze chemical reactions, it would be more advantageous to look at stainless steel reactions.

The RGE-051 debris was not analyzed for either of the ball bearing materials. The reason is that various researchers have conducted XPS analysis for molybdenum disulfide coatings such as Peng et al., Zabinski et al., Hamilton et al., and Hu et al. [53, 54, 55, 56].

CHAPTER V

CONCLUSIONS AND FUTURE RECOMMENDATIONS

The friction and wear behavior of carbon based and molybdenum disulfide based solid lubricant coatings were investigated using a high temperature pin-on-disc tribometer at various test conditions. These test conditions included atmospheric, high humidity parameters, and high temperature, low pressure, and low humidity parameters. The test materials consisted of s disc shaped tungsten carbide substrate, coated with either Perma-Slik® RGAC, or Perma-Slik® RGE-051.The materials were tested against stainless steel and tungsten carbide ball bearings. The results of this research showed that the difference in friction performance for the carbon based solid lubricant at severe conditions was significant. As a result of decrease in moisture, the carbon based lubricant will not provide lubricating effects that will be seen at moist conditions. The predominant wear mechanism was found to be abrasive wear. At elevated temperatures, oxidation was found which sped up the wear process.

As a comparison, the molybdenum disulfide solid lubricant performed equally well under both atmospheric and severe conditions. Analysis showed that there was abrasive wear present on the samples, but the lubricating effects of the molybdenum disulfide structure were dominant. Unlike the carbon based lubricant, the lack of moisture did not significantly affect performance.

This research will have impacts in the design and development of solid lubricants for aerospace applications, as well as other industries requiring the use of high

performance solid lubricants. This research will contribute to the future development of solid lubricants that must perform in extreme operating conditions.

Since the carbon based solid lubricant did not perform well at the severe conditions described in this research, it would be advised to make modifications to this coating so that it may perform better. These modifications are not limited to, but may include adding inhibitors which absorb and retain moisture, and alloying with other compounds. The molecular structure of this coating would need to be further studied in order to create a more effective lubricant.

In addition, experiment at much higher vacuum conditions must also be performed to further evaluate the coating. If experiments can be conducted at several vacuum levels, a better understanding of the coatings performance can be obtained.

REFERENCES

[1] Williams, J. A., 2005, *Engineering Tribology,* Volume 10, Cambridge University Press, Cambridge, England.

[2] Kelly, K., 2009, *Early Civilizations: Prehistoric Times to 500 C.E.*, Infobase Publishing, New York.

[3] Mang, T., and Dresel,W., 2007, *Lubricants and Lubrication*, Wiley-VCH, Zurich, Germany.

[4] Heaton, C. M., 2004, *Leonardo da Vinci and His Works: Consisting of a Life of Leonardo da Vinci*, Kessinger Publishing, Whitefish, Montana.

[5] Seirig, A., 1998, *Friction and Lubrication in Mechanical Design*, Marcel Dekker, New York.

[6] Bhushan, B., 1999, *Principles and Applications of Tribology*, Wiley-Interscience, New York.

[7] Jurgen, H., and Kappl, M., 2010, *Surface and Interfacial Forces*, Wiley-VCH, Zurich, Germany.

[8] Marinescu, I., and Dimitrov, B., 2005, *Tribology of Abrasive Machining Processes*, William Andrew, New York.

[9] Gohar, R., and Rahnejat, H., 2008, *Fundamentals of Tribology*, Imperial College Press, Covent Garden, London.

[10] Dowson, D., 1998, *History of Tribology,* 2nd Edition*,* Wiley, Hoboken, New Jersey.

[11] Stachowiak, G. W., 2005, *Wear: Materials, Mechanisms and Practice*, John Wiley and Sons, West Sussex, England.

[12] Buckley, D. H., 1981, *Surface Effects in Adhesion, Friction, Wear, and Lubrication*, Tribology Series 5. Elsevier, New York.

[13] Bayer, R. G., 2004, *Engineering Design for Wear*, CRC Press, Bellevue, Washington.

[14] Fischer, and Bobzin, K., 2009, *Friction, Wear and Wear Protection*, Wiley-VCH, Zurich, Germany.

[15] Lipkowitz, and Cundari, T. R., 2007, *Reviews in Computational Chemistry,* Volume 25, Wiley- VCH, Zurich, Germany.

[16] Mortier, R. M., Fox, M. F., and Orszulik, S. T., 2009, *Chemistry and Technology of Lubricants.* 3rd Edition, Springer, New York.

[17] You, Z., Kiyoshi, H., Yukihiko, Y., and Shuzo, K., 2003, "Tribological Properties of Silicon Carbide and Silicon Carbide- Graphite Composite Ceramics in Sliding Contact," Journal of the American Ceramic Society, **86**, pp. 991-1002.

[18] Cuong, P. D., Ahn, H. S., Yoon, E. S., and Shin, K.H., 2006, "Effects of relative humidity on tribological properties of boron carbide coating against steel," Surface and Coatings Technology, **201**, pp 4230-4235.

[19] Pirro, D., Wessol, A., and George W., 2001, *Lubrication Fundamentals*, Marcel Dekker, New York.

[20] Jacobson, B., 2003, "The Stribeck memorial lecture," Tribology International, **36**, pp. 781-789.

[21] Czichos, H., Saito, T., and Smith, L., 2006, *Springer Handbook of Materials Measurment Methods*, Springer, New York.

[22] Childs, P. R., 2004, *Mechanical Design,* 2nd Edition, Elsevier, Oxford, England.

[23] Khonsari, M. M., and Booser, R. E., 2001, *Applied Tribology: Bearing Design and Lubrication*, Wiley-Interscience, New York.

[24] Szeri, A. Z., 2005, *Fluid Film Lubrication: Theory and Design*, Cambridge University Press, Cambridge, England.

[25] Seireg, A., 1998, *Friction and Lubrication in Mechanical Design*, Marcel Dekker, New York.

[26] Frene, J., and Nicolas, D., 1997, *Hydrodynamic Lubrication: Bearings and Thrust Bearings*, Tribology Series 33, Elsevier, Oxford, England.

[27] Archbutt, L., and Richard M. D., 2010, *Lubrication and Lubricants: A Treatise on the Theory and Practice of Lubrication, and on the Nature, Properties, and Testing of Lubricants*, Nabu Press, Charleston, South Carolina.

[28] Bekir S. U., 2010, "Tribological Behaviors of Polymer-based Particle-reinforced PTFE Composite Bearings," Journal of Reinforced Plastics & Composites, **29**, pp. 1353-1358.

[29] Ohino, N., Mia, S., Morita, S., and Obara, S., 2010, "Friction and Wear Characteristics of Advanced Space Lubricants," Tribology Transactions, **53**, pp. 249-255.

[30] Steele, A., McCubbin, F.M., Fries, M., Glamoclija, M., Kater, L., and Nekvasil, H., 2010 "Graphite in an Apollo 17 Impact Melt Breccia," Science, **329**, pp. 51-55.

[31] ASTM Book of Standards, 2010, *Wear and Erosion: Vol. G 99-05*. ASTM International, West Conshocken, Pennsylvania.

[32] Everlube Products, 2007, *Perma-Slik RGAC: Fast Dry, Graphite Solid Film Lubricant*, Technical Data, Peachtree, Georgia.

[33] Everlube Products, 2007, *Perma-Slik RGE-051: Air Dry, WS2 Solid Film Lubricant*, Technical Data, Peachtree, Georgia.

[34] Soboyejo, W. O., 2003, *Mechanical Properties of Engineered Materials*, Marcel Dekker, New York.

[35] Bhushan, B., 1999, *Principles and Applications of Tribology*, John Wiley & Sons, New York.

[36] Ohmae, N., 2006, "Humidity effects on tribology of advanced carbon materials," Tribology International, **39**, pp. 1497-1502.

[37] Bhushan, B., 2002, *Introduction to Tribology*, John Wiley and Sons, New York.

[38] Dudder, G.J., Zhao, X., Krick, B., Sawyer, W. G., and Perry, S. S., 2011, "Environmental effects on the Tribological and Microstructure of MoS2–Sb2O3–C Films," Tribology Letters, **42**, pp. 203-213.

[39] Kaur, R. G., Higgs, C. F., and Heshmat, H., 2001, "Pin-on-disc tests of Pelletized Molybdenum Disulfide," Tribology Transactions, **44**, pp. 79-87.

[40] Retrieved from: http://www.keyence.com/products/microscope/microscope/vhx600/vhx600_features _1.php;May 28, 2011. (Keyence Corporation, Osaka, Japan, 2011)

[41] Blau, P. J., and Jun, Q., 2006, "An Efficient Method for Accurately Determining Wear Volumes of Sliders with Non-Flat Wear Scars and Compound Curvatures," Wear, **261**, pp. 848-855.

[42] Blau, P. J., 2009, *Friction Science and Technology: From Concepts to Applications*, CRC Press, Boca Raton.

[43] Johnson, K. L., 1987, *Contact Mechanics*, Cambridge University Press, New York.

[44] Jun, Q., and Truhan, J. J., 2006. "An efficient method for accurately determining wear volumes with non-flat wear scars and compound curvatures," Wear, **261**, pp. 848-855.

[45] Blau, P. J., 2001, "The significance and use of the friction coefficient," Tribology International, **34**, pp. 585-591.

[46] Bregliozzi, G., Di Schino, A., Kenny, J.M., and Haefke, H., 2003, "The influence of atmospheric humidity and grain size on the friction and wear of AISI 304 austenitic stainless steel," Materials Letters, **57**, pp. 4505-4508.

[47] Konca, E., Cheng, Y.T., Weiner, A.M., Dasch, J.M., and Alpas, A.T., 2005, "Effect of test atmosphere on the tribological behavior of the non-hydrogenated diamond-like carbon coatings against 319 aluminum alloy and tungsten carbide," Surface & Coatings Technology, **200**, pp. 1783-1791.

[48] Mendez, A., Santamaria, R., Granda, M., and Menendez, R., 2008, "The effect of graphite on the mechanical and tribological properties of pitch-based granular carbon composites," Journal of Material Science, **43**, pp. 4541-4549.

[49] Tsujikawa, M., Nagamine, K., Ikenaga, A., and Hino, M., 2008, "Influence of graphite morphology on dry sliding wear of flake graphite cast irons," International Journal of Cast Metals Research, **20**, pp 1-4.

[50] Garratt-Reed, A. J., and Bell, D. C., 2003, *Energy Dispersive X-Ray Analysis in the Electron Microscope*, BIOS Scientific Publishers Ltd., New York.

[51] Liu, Y., Erdemir, A., and Meletis, E. I., 1996, "A study of the wear mechanism of diamond-like carbon films," Surface and Coatings Technology, **82**, pp. 48-56.

[52] Wagner, J.M., 2010, *X-Ray Photoelectron Spectroscopy: Chemical Engineering Methods and Technology*, Nova Science Publishers Inc., New York.

[53] Peng, Z., Xiao, W., Xiao-Dong, W., Pei, H., and Jun, S., 2006, "Tribology performances of molybdenum disulfide reinforced thermoplastic polymers under dry and water lubrication conditions," Industrial Lubrication and Tribology, **58**, pp. 195-201.

[54] Zabinski, J. S., Bultman, J. E., Sanders, J. H., and Hu, J .J., 2006, "Multi-environmental lubrication performance and mechanism of MoS2/Sb2O3/C composite films," Tribology Letters, **23**, pp. 155-163.

[55] Hamilton, M. A., Alvarez, L. A., Mauntler, N. A., Argibay, N., Colbert, R., Burris, L. D., Muratore, C., Voevodin, A. A., Perry, S. S., and Sawyer, W. G., 2008, "A possible link between macroscopic wear and dependent friction behaviors of MoS2 coatings," Tribology Letters, **32**, pp. 91-98.

[56] Hu, X., 2005, "On the size effect of molybdenum disulfide particles on tribological performance," Industrial Lubrication and Tribology, **57**, pp. 255-259.

VITA

Name: Carlos Joel Sanchez

Address: 100B Engineering/Physics Building, 3123 TAMU

                          College Station, TX 77840

Email Address: carlos.joel.sanchez@gmail.com

Education: B.S., Mechanical Engineering, Texas A&M University, 2009

                          M.S., Mechanical Engineering, Texas A&M University, 2011